# Contents

# Chapter 15

# Turbulence

Version 1015.1.K, 4 February 2009
*Please send comments, suggestions, and errata via email to kip@caltech.edu, or on paper to Kip Thorne, 350-17 Caltech, Pasadena CA 91125*

**Box 15.1**
**Reader's Guide**

- This chapter relies heavily on Chaps. 12 and 13.
- The remaining chapters on fluid mechanics and magnetohydrodynamics (Chaps. 15–18) do not rely significantly on this chapter, nor do any of the remaining chapters in this book.

## 15.1 Overview

In Sec. 12.7.6, we derived the Poiseuille formula for the flow of a viscous fluid down a pipe by assuming that the flow is laminar, i.e. that it has a velocity parallel to the pipe wall. We showed how balancing the stress across a cylindrical surface led to a parabolic velocity profile and a rate of flow proportional to the fourth power of the pipe diameter, $d$. We also defined the Reynolds number; for pipe flow it is $R_d \equiv \bar{v}d/\nu$, where $\bar{v}$ is the mean speed in the pipe. Now, it turns out experimentally that the flow only remains laminar up to a critical Reynolds number that has a value in the range $\sim 10^3 - 10^5$ depending upon the smoothness of the pipe's entrance and roughness of its walls. If the pressure gradient is increased further (and thence the mean speed $\bar{v}$ and Reynolds number $R_d$ are increased), then the velocity field in the pipe becomes irregular both temporally and spatially, a condition known as *turbulence*.

Turbulence is common in high Reynolds number flows. Much of our experience of fluids involves air or water for which the kinematic viscosities are $\sim 10^{-5}$ and $10^{-6}$ m$^2$ s$^{-1}$ respectively. For a typical everyday flow with a characteristic speed of $v \sim 10$ m s$^{-1}$ and a characteristic length of $d \sim 1$m, the Reynolds number is huge: $R_d = vd/\nu \sim 10^6 - 10^7$. It is

therefore not surprising that we see turbulent flows all around us. Smoke in a smokestack, a cumulus cloud and the wake of a ship are three examples.

In Sec. 15.2 we shall illustrate the phenomenology of the transition to turbulence as $R_d$ increases using a particularly simple example, the flow of a fluid past a circular cylinder oriented perpendicular to the line of sight. We shall see how the flow pattern is dictated by the Reynolds number and how the velocity changes from steady creeping flow at low $R_d$ to fully-developed turbulence at high $R_d$.

What *is* turbulence? Fluid dynamicists can certainly recognize it but they have a hard time defining it precisely,[1] and an even harder time describing it quantitatively.

At first glance, a quantitative description appears straightforward. Decompose the velocity field into Fourier components just like the electromagnetic field when analysing electromagnetic radiation. Then recognize that the equations of fluid dynamics are nonlinear, so there will be coupling between different modes (akin to wave-wave coupling between light modes in a nonlinear crystal, discussed in Chap. 9). Analyze that coupling perturbatively. The resulting *weak-turbulence theory* (some of which we sketch in Sec. 15.3 and Ex. 15.3) is useful when the turbulence is not too strong. In this theory, among other things, one averages the spectral energy density over many realizations of a stationary turbulent flow to obtain a mean spectral energy density for the fluid's motions. Then, if this energy density extends over several octaves of wavelength, scaling arguments can be invoked to infer the shape of the energy spectrum. This produces the famous *Kolmogorov spectrum* for turbulence. This spectrum has been verified experimentally under many different conditions. (Another weak-turbulence theory which is developed along similar lines is the *quasi-linear* theory of nonlinear plasma interactions, which we shall develop in Chap. 22.)

Most turbulent flows come under the heading of *fully developed* or *strong turbulence* and cannot be well described in this weak-turbulence manner. Part of the problem is that the $(\mathbf{v}\cdot\nabla)\mathbf{v}$ term in the Navier-Stokes equation is a strong nonlinearity, not a weak coupling between linear modes. As a consequence, eddies of size $\ell$ persist for typically no more than one turnover timescale $\sim \ell/v$ before they are broken up, and so do not behave like weakly coupled normal modes. Another, related, problem is that it is not a good approximation to assume that the phases of the modes are random, either spatially or temporally. If we look at a snapshot of a turbulent flow, we frequently observe large, well-defined coherent structures like eddies and jets, which suggests that the flow is more organized than a purely random superposition of modes, just as the light reflected from the surface of a painting differs from that emitted by a black body. Moreover, if we monitor the time variation of some fluid variable, such as one component of the velocity at a given point in the flow, we can recognize *intermittency* – the irregular starting and ceasing of strong turbulence. Again, this is such a marked effect that there is more than a random-mode superposition at work, reminiscent of the distinction between noise and music (at least some music). Strong turbulence is therefore not just a problem in perturbation theory; and alternative, semiquantitative approaches must be devised.

In the absence of a decent quantitative theory, it becomes necessary to devise intuitive, qualitative and semiquantitative approaches to the *physical* description of turbulence (Secs. 15.3 and 15.4). We emphasize the adjective physical, because our goal is not just to produce

[1]The analogy to Justice Potter Stewart's definition of pornography should be resisted.

empirical descriptions of the consequences of turbulence, but rather to comprehend the underlying physical character of turbulence, going beyond purely empirical rules on one hand and uninstructive mathematical expansions on the other. This means that the reader must be prepared to settle for order of magnitude scaling relations based on comparing the relative magnitudes of individual terms in the governing fluid dynamical equations. At first, this will seem quite unsatisfactory. However, much contemporary physics has to proceed with this methodology. It is simply too hard, in turbulence and some other phenomena, to discover elegant mathematical counterparts to the Kepler problem or the solution of the Schrödinger equation for the hydrogen atom.

A good example of a turbulent flow that embodies some of these principles is a turbulent boundary layer along a solid surface (Sec. 15.4). Turbulent boundary layers generally exert more shear stress on a surface than laminar boundary layers, but nevertheless usually produce less total drag, because they are less prone to separation from the surface when subjected to an adverse pressure gradient. For this reason, turbulence is often induced artificially in boundary layers, e.g. those going over the top of an airplane wing, or those on one face of a ball. In Sec. 15.4 we shall study the structure of a turbulent boundary layer and briefly discuss how its turbulence can arise through instability of a laminar boundary layer; and we shall examine some applications to balls moving through the air (golf balls, cricket balls, baseballs, ...).

Whether or not a flow becomes turbulent can have a major influence on how fast chemical reactions occur in liquids and gases; this is another motivation for artificially inducing or surpressing turbulence.

One can gain additional insight into turbulence by a technique that is often useful when struggling to understand complex physical phenomena: Replace the system being studied by a highly idealized model system that is much simpler than the original one, both conceptually and mathematically, but that retains at least one central feature of the original system. Then analyze the model system completely, with the hope that the quantitative insight so gained will be useful in understanding the original problem. This approach is central, e.g., to research in quantum cosmology, where one is trying to understand how the initial conditions for the expansion of the universe were set, and to do so one works with model universes that have only a few degrees of freedom. Similarly, during the 1970's and especially the 1980's and 1990's, new insights into turbulence came from studying idealized *dynamical systems* that have very small numbers of degrees of freedom, but have the same kinds of nonlinearities as produce turbulence in fluids. We shall examine several such low-dimensional dynamical systems and the insights they give in Sec. 15.5.

The most useful of those insights deal with the onset of weak turbulence, and the fact that it seems to have much in common with the onset of *chaos* (irregular and unpredictable dynamical behavior) in a wide variety of other dynamical systems — e.g., coupled pendula, electric circuits, and planets, asteroids, satellites and rings in the solar system. A great discovery of modern classical physics/mathematics has been that there exist organizational principles that govern the behavior of these seemingly quite different chaotic physical systems. In Sec. 15.5 we shall discuss some very simple models for the onset of chaos and shall outline the relationship of those models to the behavior of turbulent fluids.

Despite these elegant modern insights, those features of turbulence that are important in

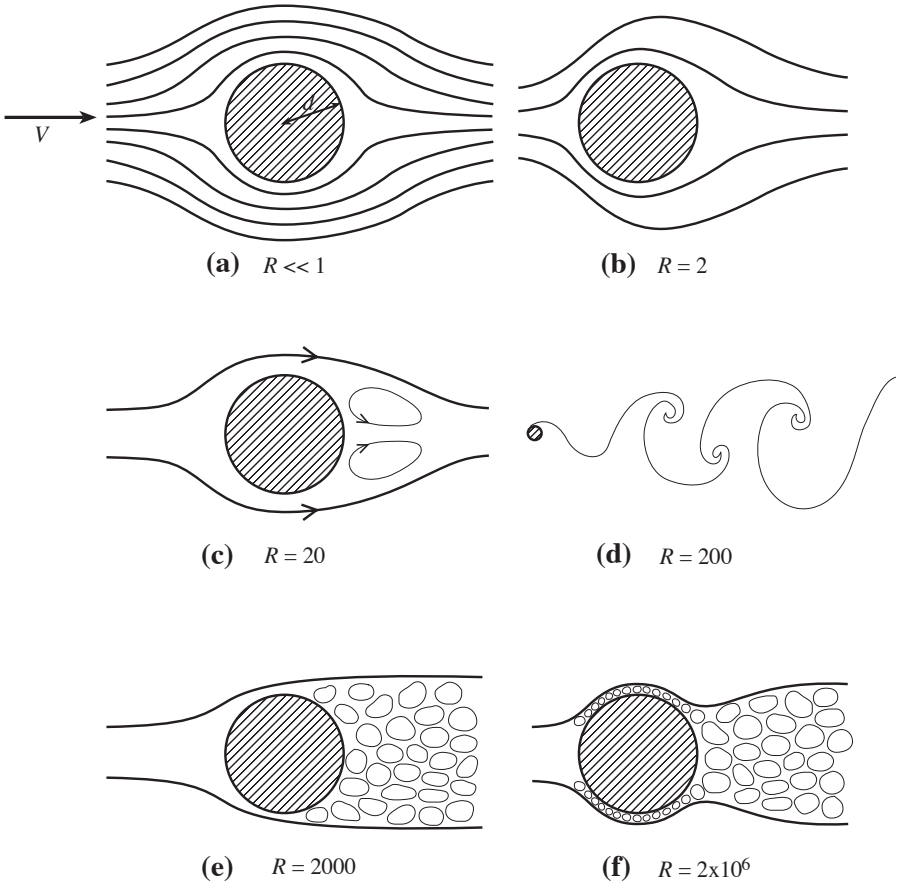


**Fig. 15.1:** Schematic depiction of flow past a cylinder for steadily increasing values of the Reynolds number $R_d = Vd/\nu$ as labeled.

practical situations, e.g. in aeronautical or marine engineering, are still described today only qualitatively and empirically. This is an indication of how far we are from a satisfactory, physical theory of turbulence.

## 15.2 The Transition to Turbulence - Flow Past a Cylinder

We illustrate qualitatively how a flow (and especially its transition to turbulence) depends on its Reynolds number by considering a specific problem, the flow of a uniformly moving fluid past a cylinder oriented transverse to the line of sight (Fig. 15.1). We assume that the velocity is very small compared with the speed of sound, so that the effects of compressibility can be ignored. Let the cylinder diameter be $d$ and choose this as the characteristic length in the problem. Similarly, let the velocity far upstream be $V$ and choose this as the characteristic

velocity so that the Reynolds number is

$$\boxed{R_d = \frac{Vd}{\nu}\ .} \tag{15.1}$$

We assume, initially, that the flow is stationary (no turbulence) as well as incompressible, and the effects of gravity are negligible. Then the equations governing the flow are incompressibility,

$$\boldsymbol{\nabla}\cdot\mathbf{v} = 0\ , \tag{15.2a}$$

and the time-independent Navier-Stokes equation (12.65) with $\partial\mathbf{v}/\partial t = 0$:

$$\mathbf{v}\cdot\boldsymbol{\nabla}\mathbf{v} = -\frac{\boldsymbol{\nabla}P}{\rho} + \nu\nabla^2\mathbf{v}\ . \tag{15.2b}$$

These four equations (one incompressibility, three components of Navier-Stokes) can be solved for the pressure and the three components of velocity subject to the velocity vanishing on the surface of the cylinder and becoming uniform far upstream.

From the parameters of the flow (the cylinder's diameter $d$, the fluid's incoming velocity $V$ and its density $\rho$ and kinematic viscosity $\nu$) we can construct only one dimensionless number, the Reynolds number $R_d = Vd/\nu$. (If the flow speed were high enough that incompressibility fails, then the sound speed $c_s$ would also be a relevant parameter and there would be a second dimensionless number, the Mach number $M = V/c_s$; Chaps. 15 and 16). With $R_d$ the only dimensionless number, we are guaranteed on dimensional grounds that the solution to the flow equations can be expressed as

$$\boxed{\mathbf{v}/V = \mathbf{U}(\mathbf{x}/d, R_d).} \tag{15.3}$$

Here $\mathbf{U}$ is a dimensionless function of the dimensionless $\mathbf{x}/d$, and it can take wildly different forms depending on the value of the Reynolds number $R_d$; cf. Fig. 15.1, which we shall discuss below.

The functional form (15.3) of $\mathbf{v}$ has important implications. If we compute the flow for specific values of the upstream velocity $V$, the cylinder's diameter $d$ and the kinematic viscosity $\nu$ and then double $V$ and $d$ and quadruple $\nu$ so $R_d$ is unchanged, then the new solution will be similar to the original solution. It can be produced from the original by rescaling the flow velocity to the new upstream velocity and the distance to the new cylinder diameter. [For this reason, Eq. (15.3) is sometimes called a *scaling relation*.] On the other hand, if we had only doubled the kinematic viscosity, the Reynolds number would have also doubled and we could be dealing with a qualitatively different flow.

In discussing the flow past the cylinder, a useful concept is the *stagnation pressure* in the upstream flow. This is the pressure the fluid would have, according to the Bernoulli Principle $v^2/2 + u + P/\rho = \text{const}$, if it were brought to rest at the leading edge of the cylinder without significant action of viscosity. Ignoring the effects of compressibility (so $u$ and $\rho$ are constant), this stagnation pressure is

$$\boxed{P_{\rm stag} = P_0 + \frac{1}{2}\,\rho V^2\ ,} \tag{15.4}$$

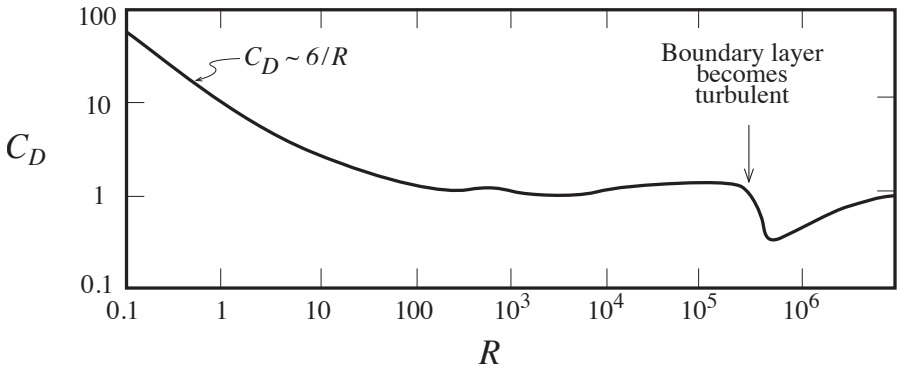


**Fig. 15.2:** Drag coefficient $C_D$ for flow past a cylinder as a function of Reynolds number $R_d = Vd/\nu$. This graph, adapted from Fig. 3.14 of Tritton (1977), is based on experimental measurements.

where $P_0$ is the upstream pressure. Suppose that this stagnation pressure were to act over the whole front face of the cylinder, while the pressure $P_0$ acted on the downstream face. The net force per unit length, $F_D$, would then be $\frac{1}{2}\rho V^2 d$. This is a first rough estimate for the drag force on the cylinder. It is conventional to define a *drag coefficient* as the ratio of the actual drag force per unit length to this rough estimate:

$$C_D \equiv \frac{F_D}{\frac{1}{2}\rho V^2 d} \,. \tag{15.5}$$

This drag coefficient, being a dimensionless feature of the flow (15.3), can depend only on the dimensionless Reynolds number $R_d$: $C_D = C_D(R_d)$; see Fig. 15.2. Similarly for flow past a body with cross sectional area $A$ perpendicular to the flow and with any other shape, the drag coefficient

$$\boxed{C_D \equiv \frac{F_{\rm drag}}{\frac{1}{2}\,\rho V^2 A}} \tag{15.6}$$

will be a function only of $R$. However, the specific functional form of $C_D(R)$ will depend on the body's shape.

Now, turn to the details of the flow around a cylinder as described in Figs. 15.1 and 15.2. At low Reynolds number, $R_d \ll 1$, there is creeping flow [Fig. 15.1(a)] just like that analyzed in detail for a spherical obstacle in Chap. 13. As you might have surmised by tackling Ex. 13.4, the details of flow past a long object such as a cylinder are subtly different from those of flow past a short one such as a sphere. This is because, for a cylinder, inertial forces become comparable with viscous and pressure forces at distances $\sim d/R_d$ where the flow is still significantly perturbed from uniform motion, while for short objects inertial forces become significant only at much larger radii, where the flow is little perturbed by the object's presence. Despite this, the flow streamlines around a cylinder at $R_d \ll 1$ are similar to those for a sphere and are approximately symmetric between upstream and downstream. The fluid is decelerated by viscous stresses as it moves past the cylinder along these streamlines and the pressure is higher on the cylinder's front face than on its back. Both effects contribute

to the net drag force acting on the cylinder. The momentum removed from the flow is added to the cylinder. At $r \ll d/R_d$ the viscous stress dominates over the fluid's inertial stress, and the fluid momentum therefore is being transferred largely to the cyclinder, at a rate per unit area $\sim \rho V^2$, while at $r \gtrsim d/R_d$ the viscous and inertial stresses are comparable and balance each other, and the flow's momentum is not being transferred substantially to the cylinder. This implies that the effective cross sectional width over which the cylinder extracts the fluid momentum is $\sim d/R_d$, and correspondingly the net drag force per unit length is $F \sim \rho V^2 d/R_d$, which implies [cf. Eq. (15.5)] a drag coefficient $\sim 1/R_d$ at low Reynolds numbers $R_d \ll 1$. A more careful analysis gives $C_D \sim 6/R_d$, as shown experimentally in Fig. 15.2.

As the Reynolds number is increased to $\sim 1$ [Fig. 15.1(b)], the effective cross section gets reduced to roughly the cylinder's geometrical width $d$, and correspondingly the drag coefficient decreases to $C_D \sim 1$. At this Reynolds number, $R_d \sim 1$, the velocity field begins to appear asymmetric from front to back.

With a further increase in $R_d$, a laminar boundary layer of thickness $\delta \sim d/\sqrt{R_d}$ starts to form. The viscous force per unit length due to this boundary layer is $F \sim \rho V^2 d/\sqrt{R_d}$ [Eqs. (13.46)–(13.48) divided by $w$, with $\ell \sim d$ and $v_o = V$]. It might therefore be thought that the drag would continue to decrease as $C_D \sim 1/\sqrt{R_d}$, when $R_d$ increases substantially above unity making the boundary layer thin and making the external flow start to resemble potential flow. However, this does *not* happen. Instead, at $R_d \sim 5$, the flow begins to separate from the back side of the cylinder and is there replaced by two retrograde eddies [Fig. 15.1(c)]. As described in Sec. 13.4.2, this separation occurs because an adverse pressure gradient $(\mathbf{v}\cdot\boldsymbol{\nabla})P > 0$ develops outside the boundary layer, near the cylinder's downstream face, and causes the separated boundary layer to be replaced by these two counter-rotating eddies. The pressure in these eddies is of order the flow's incoming pressure $P_0$ and is significantly less than the stagnation pressure $P_{\rm stag} = P_0 + \frac{1}{2}\rho V^2$ at the cylinder's front face, so the drag coefficient stabilizes at $C_D \sim 1$.

As the Reynolds number increases above $R_d \sim 5$, the size of the two eddies increases until, at $R_d \sim 100$, the eddies are shed dynamically, and the flow becomes non-stationary. The eddies tend to be shed alternately in time, first one and then the other, producing a pattern of alternating vortices downstream known as a *Karman vortex street* [Fig. 15.1(d)].

When $R_d \sim 1000$, the downstream vortices are no longer visible and the wake behind the cylinder contains a velocity field irregular on all scales [Fig. 15.1(e)]. This downstream flow has become turbulent. Finally, at $R_d \sim 3\times 10^5$, the boundary layer, which has been laminar up to this point, itself becomes turbulent [Fig. 15.1(f)], reducing noticeably the drag coefficient (Fig. 15.2). We shall explore the cause of this reduction below. [The physically relevant Reynolds number for onset of turbulence in the boundary layer is that computed not from the cylinder diameter $d$, $R_d = Vd/\nu$, but rather from the boundary layer thickness $\delta \sim d/R_d^{1/2}$:

$$\boxed{R_\delta = \frac{V\delta}{\nu} \sim \frac{V d R_d^{-1/2}}{\nu} = \sqrt{R_d}\,.} \tag{15.7}$$

The onset of boundary-layer turbulence is at $R_\delta \sim \sqrt{3\times 10^5} \sim 500$, about the same as the $R_d \sim 1000$ for onset of turbulence in the wake.]

An important feature of this changing flow pattern is the fact that at $R_d \ll 1000$ [Figs. 15.1(a)–(d)], before any turbulence sets in, the flow (whether steady or dynamical) is translation symmetric; i.e., it is independent of distance $z$ down the cylinder; i.e., it is two-dimensional. This is true even of the Karman vortex street. By contrast, the turbulent velocity field at $R_d \gtrsim 1000$ is fully three-dimensional. At these large Reynolds numbers, small, non-translation-symmetric perturbations of the translation-symmetric flow grow into vigorous, three-dimensional turbulence. This is a manifestation of the fact (which we shall explore below) that two-dimensional flows cannot exhibit true turbulence. True turbulence requires chaotic motions in all three dimensions.

The most important feature of this family of flows, a feature that is characteristic of most such families, is that there is a critical Reynolds number for the onset of turbulence. That critical number can range from $\sim 30$ to $\sim 10^5$, depending on the geometry of the flow and on precisely what length and speed are used to define the Reynolds number.

**********

## EXERCISES

**Exercise 15.1** *Example: Spreading of a laminar wake*
Consider stationary, incompressible flow around a long circular cylinder with diameter $d$, extending perpendicular to the velocity. Let the flow far in front of the cylinder be uniform with speed $V$. Let the Reynolds number $R_d$ be small enough for the flow to remain laminar. (We will treat the turbulent regime at higher $R_d$ in Ex. 15.4 below.) Behind the body is a wake with width $w(x)$, at a distance $x$ downstream from the cylinder. At the center of the wake, the flow speed is reduced to $V - \Delta v$, where $\Delta v$ is called the *velocity deficit*.

(a) Use momentum conservation to derive the approximate relationship $\Delta v \propto w^{-1}$ between the velocity deficit and the width of the wake at a distance $x$ far downstream from the cylinder. Then use the Navier-Stokes equation and invoke self similarity (like that of the Blasius profile in Sec. 13.4) to show that $\Delta v \propto x^{-1/2}$.

(b) How will this scaling law be modified if we replace the cylinder by a sphere?

**Exercise 15.2** *Example: Spreading of Laminar Jets*
Consider a narrow, two-dimensional, incompressible (i.e. subsonic) jet emerging from a two-dimensional nozzle into ambient fluid of the same composition and pressure, at rest. (By two-dimensional we mean that the nozzle and jet are translation symmetric in the third dimension.) Let the Reynolds number be low enough for the flow to be laminar; we shall study the turbulent regime in Ex. 15.5 below. We want to understand how rapidly this laminar jet spreads.

(a) Show that the pressure forces far downstream from the nozzle are likely to be much smaller than the viscous forces and can therefore be ignored.

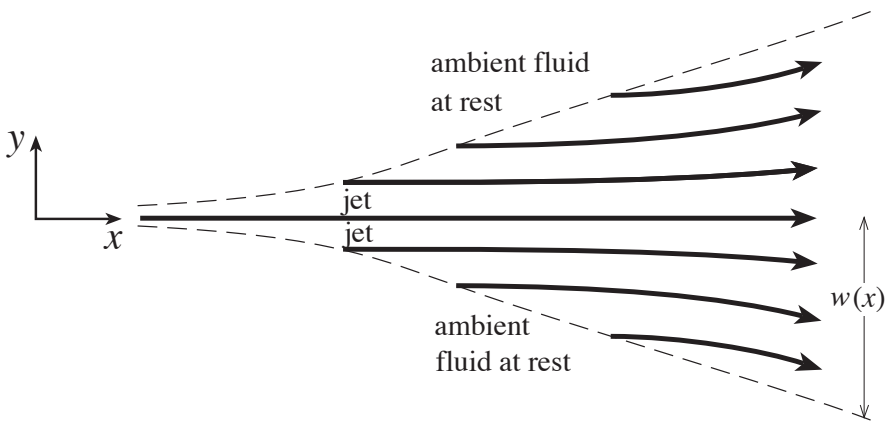


**Fig. 15.3:** Two-dimensional laminar jet. As the jet widens, it entrains ambient fluid.

(b) Let the jet's thrust per unit length (i.e. the momentum per unit time per unit length flowing through the nozzle) be $\mathcal{F}$. Introduce cartesian coordinates $x, y$, with $x$ parallel to and $y$ perpendicular to the jet (cf. Fig. 15.3). Use the Navier-Stokes equation to make an order of magnitude estimate of the speed $v_x$ and the width $w$ of the jet as a function of distance $x$ downstream in a similar manner to the previous problem.

(c) Use these scalings to modify the self-similarity analysis that we used for the laminar boundary layer in Sec. 13.4, and thereby obtain the following approximate solution for the jet velocity profile:

$$v_x = \left(\frac{3\mathcal{F}^2}{32\rho^2\nu x}\right)^{1/3} \mathrm{sech}^2\left(\left[\frac{\mathcal{F}}{48\rho\nu^2x^2}\right]^{1/3} y\right) . \tag{15.8}$$

**********

## 15.3 Semi-Quantitative Analysis of Turbulence

### 15.3.1 Weak Turbulence

The considerations of the last section motivate us to attempt to construct a semi-quantitative, mathematical description of turbulence. We shall begin with an approach that is moderately reasonable for weak turbulence, but becomes much less so when the turbulence is strong. (In Sec. 15.3.4 below, we shall develop a model for turbulence based on interacting eddies. One can regard the turbulence as weak if the timescale $\tau_*$ for a big eddy to feed most of its energy to smaller eddies is long compared to the eddy's turnover time $\tau$, i.e., its "rotation period". Unfortunately, turbulence is usually strong, so the eddy's energy loss time is of order its turnover time, $\tau_* \sim \tau$, which means the eddy loses its identity in roughly one turnover time. For such strong turbulence, the weak-turbulence formalism that we shall sketch here is only semiquantitatively accurate.)

The theory of weak turbulence (with gravity negligible and the flow very subsonic so it can be regarded as incompressible) is based on the standard incompressibility equation and the time-dependent Navier-Stokes equation, which we write in the following forms:

$$\boldsymbol{\nabla}\cdot\mathbf{v} = 0\ , \tag{15.9a}$$

$$\rho\frac{\partial\mathbf{v}}{\partial t} + \boldsymbol{\nabla}\cdot(\rho\mathbf{v}\otimes\mathbf{v}) = -\boldsymbol{\nabla}P + \rho\nu\nabla^2\mathbf{v}\ . \tag{15.9b}$$

[Eq. (15.9b) is equivalent to (15.2b) with $\partial\mathbf{v}/\partial t$ added because of the time dependence, and with the inertial force term rewritten via $\boldsymbol{\nabla}\cdot(\rho\mathbf{v}\otimes\mathbf{v}) = \rho(\mathbf{v}\cdot\boldsymbol{\nabla})\mathbf{v}$, or equivalently in index notation, $(\rho v_i v_j)_{;i} = \rho_{,i}v_i v_j + \rho(v_{i;i}v_j + v_i v_{j;i}) = \rho v_i v_{j;i}$ .] Equations (15.9a) and (15.9b) are four scalar equations for four unknowns, $P(\mathbf{x},t)$ and the three components of $\mathbf{v}(\mathbf{x},t)$; $\rho$ and $\nu$ can be regarded as constants in these equations.

To obtain the weak-turbulence versions of these equations, we split the velocity field $\mathbf{v}(\mathbf{x},t)$ and pressure $P(\mathbf{x},t)$ into steady parts $\bar{\mathbf{v}}$, $\bar{P}$, plus fluctuating parts, $\delta\mathbf{v}$, $\delta P$:

$$\boxed{\mathbf{v} = \bar{\mathbf{v}} + \delta\mathbf{v}\ ,\quad P = \bar{P} + \delta P\ .} \tag{15.10}$$

We can think of (or, in fact, define) $\bar{\mathbf{v}}$ and $\bar{P}$ as the time averages of $\mathbf{v}$ and $P$, and define $\delta\mathbf{v}$ and $\delta P$ as the difference between the exact quantities and the time-averaged quantities.

The time-averaged variables $\bar{\mathbf{v}}$ and $\bar{P}$ are governed by the time averages of the incompressibility and Navier-Stokes equations (15.9). Because the incompressibility equation is linear, its time average

$$\boxed{\boldsymbol{\nabla}\cdot\bar{\mathbf{v}} = 0} \tag{15.11a}$$

entails no coupling of the steady variables to the fluctuating variables. By contrast, the nonlinear inertial term $\boldsymbol{\nabla}\cdot(\rho\mathbf{v}\otimes\mathbf{v})$ in the Navier-Stokes equation gives rise to such a coupling in the (time-independent) time-averaged equation:

$$\boxed{\rho(\bar{\mathbf{v}}\cdot\boldsymbol{\nabla})\bar{\mathbf{v}} = -\boldsymbol{\nabla}\bar{P} + \nu\rho\nabla^2\bar{\mathbf{v}} - \boldsymbol{\nabla}\cdot\mathbf{T}_R\ .} \tag{15.11b}$$

Here

$$\boxed{\mathbf{T}_R \equiv \rho\overline{\delta\mathbf{v}\otimes\delta\mathbf{v}}} \tag{15.11c}$$

is known as the *Reynolds stress tensor*. It serves as a "driving term" in the time-averaged Navier-Stokes equation (15.11b) — a term by which the fluctuating part of the flow acts back on, and influences the time-averaged flow.

This Reynolds stress $\mathbf{T}_R$ can be regarded as an additional part of the total stress tensor, analogous to the gas pressure computed in kinetic theory,[2] $P = \frac{1}{3}\rho\overline{v^2}$, where $v$ is the molecular speed. $\mathbf{T}_R$ will be dominated by the largest eddies present, and it can be anisotropic, especially when the largest-scale turbulent velocity fluctuations are distorted by interaction with an averaged shear flow, i.e when $\bar{\sigma}_{ij} = \frac{1}{2}(\bar{v}_{i;j} + \bar{v}_{j;i})$ is large.

If the turbulence is both stationary and homogeneous (a case we shall specialize to below when studying the "Kolmogorov spectrum"), then the Reynolds stress tensor can be written

[2]Deducible from Eq. (2.35c) or from Eqs. (2.37b) and (2.37c) with mean energy per particle $\bar{E} = \frac{1}{2}m\overline{v^2}$.

in the form $\mathbf{T}_R = P_R\mathbf{g}$, where $P_R$ is the Reynolds pressure, which is independent of position, and $\mathbf{g}$ is the metric, so $g_{ij} = \delta_{ij}$. In this case, the turbulence will exert no force density on the mean flow; i.e., $\boldsymbol{\nabla}\cdot\mathbf{T}_R = \boldsymbol{\nabla}P_R$ will vanish in the time-averaged Navier-Stokes equation (15.11b). By contrast, near the edge of a turbulent region (e.g., near the edge of a turbulent wake or jet or boundary layer), the turbulence will be inhomogeneous, and thereby (as we shall see in the next subsection) will exert an important influence on the time-independent, averaged flow.

Notice that the Reynolds stress tensor is the tensorial *auto-correlation* function of the velocity fluctuation field (multiplied by density $\rho$). It is possible to extend this "theory" of weak turbulence with the aid of a *cross-correlation* of the velocity field. The cross-correlation function involves taking the time average of products of velocity components (or other relevant physical quantities) at different points simultaneously, or at the same point at different times. (It is relatively straightforward experimentally to measure these correlation functions.) As we discuss in greater detail below (and as we also saw for one-dimensional random processeses in Sec. 5.3 and for multidimensional, complex random processes in Ex. 8.7), the Fourier transforms of these correlation functions give the spatial and temporal spectral densities of the fluctuating quantities.

Just as the structure of the time-averaged flow is governed by the time-averaged incompressibility and Navier-Stokes equations (15.11) (with the fluctuating variables acting on the time-averaged flow through the Reynolds stress), so also the fluctuating part of the flow is governed by the fluctuating (difference between exact and time-averaged) incompressibility and Navier-Stokes equations; see Ex. 15.3.

### 15.3.2 Turbulent Viscosity

Additional tools that are often introduced in the theory of weak turbulence come from taking the analogy with the kinetic theory of gases one stage further and defining *turbulent transport coefficients* (most importantly a turbulent viscosity that governs the turbulent transport of momentum). These turbulent transport coefficients are derived by simple analogy with the kinetic-theory transport coefficients (Sec. 2.7.) Momentum, heat, etc. are transported most efficiently by the largest turbulent eddies in the flow; therefore, in estimating the transport coefficients we replace the particle mean free path by the size $\ell$ of the largest eddies and the mean particle speed by the magnitude $v_\ell$ of the fluctuations of velocity in the largest eddies. The result, for momentum transport, is a model turbulent viscosity

$$\boxed{\nu_t \simeq \frac{1}{3} v_\ell \ell} \tag{15.12}$$

[cf. Eq. (12.72) for molecular viscosity, with $\nu = \eta/\rho$]. The Reynolds stress is then approximated as a turbulent shear stress of the standard form

$$\boxed{\mathbf{T}_R \simeq -2\rho\nu_t\bar{\boldsymbol{\sigma}}\ .} \tag{15.13}$$

Here $\bar{\boldsymbol{\sigma}}$ is the rate of shear tensor (12.63b) evaluated using the mean velocity field $\bar{\mathbf{v}}$. Note that the turbulent kinematic viscosity defined in this manner, $\nu_t$, is a property of the turbulent flow and not an intrinsic property of the fluid; it differs from molecular viscosity in this important respect.

By considerations similar to these for turbulent viscosity, one can define and estimate a turbulent thermal conductivity for the spatial transport of time-averaged heat (cf. Sec. 2.7.2) and a turbulent diffusion coefficient for the spatial transport of one component of a time-averaged fluid through another, for example an odor crossing a room (cf. Ex. 2.19).

In Ex. 15.4 we shall see how the Reynolds stress (15.13), expressed in terms of the turbulent viscosity, produces (via vortex-line diffusion) the spatial widening of the time-averaged, turbulent wake behind a cylinder, and in Ex. 15.5 we shall see it for a turbulent jet.

In the case of a gas, $\nu_t$ and the other turbulent transport coefficients can be far far larger than their kinetic-theory values. For example, air in a room subject to typical uneven heating and cooling might circulate with an average largest eddy velocity of $v_\ell \sim 1$ cm s$^{-1}$ and an associated eddy size of $\ell \sim 3$ m. (This can be estimated by observing the motion of illuminated dust particles.) The kinematic turbulent viscosity $\nu_t$ — and also the turbulent diffusion coefficient $D_t$ (Ex. 2.19) — associated with these motions are $\nu_t \sim D_t \sim 10^{-2}$ m$^2$ s$^{-1}$, some three orders of magnitude larger than the molecular values. Correspondingly, a time-averaged turbulent wake (or boundary layer or jet) will widen, downstream, due to diffusion of time-averaged vorticity, much more rapidly than will its laminar counterpart.

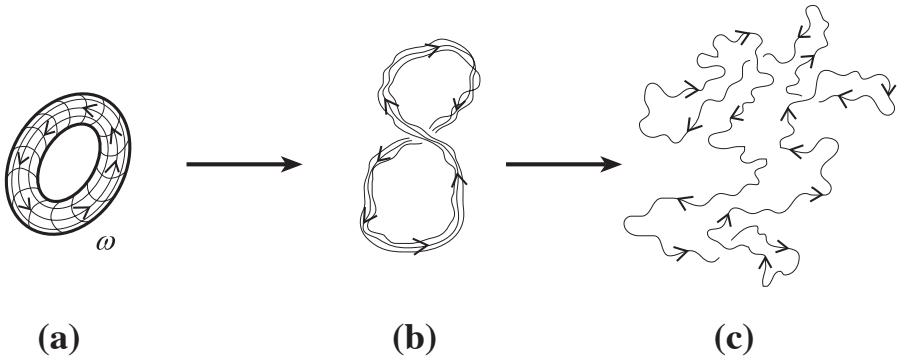


**Fig. 15.4:** Schematic illustration of the propagation of turbulence by the stretching of vortex lines. The tube of vortex lines in (a) gets stretched and thereby is forced into a reduced cross section by the turbulent evolution from (a) to (b) to (c). The reduced cross section means an enhanced vorticity on smaller scales.

### 15.3.3 Relationship to Vorticity

Three-dimensional turbulent flows contain tangled vorticity. As we discussed in Chap. 13, vortex lines move with the fluid and can be stretched by the action of neighboring vortex lines. As a bundle of vortex lines is stretched and twisted (Fig. 15.4), the incompressibility of the fluid causes the bundle's cross section to decrease and correspondingly causes the magnitude of its vorticity to increase, and the lengthscale on which the vorticity changes to decrease (cf. Sec. 13.2). The continuous lengthening and twisting of the fluid therefore creates vorticity on progressively smaller length scales.

Note that, when the flow is two-dimensional (i.e. translation symmetric), there is no stretching of the vortex lines and thus no inexorable driving of the turbulent energy to

smaller and smaller length scales. This is one reason why true turbulence does not occur in two dimensions, only in three.

### 15.3.4 Kolmogorov Spectrum for Homogeneous and Isotropic Turbulence

When a fluid exhibits turbulence over a large volume that is well-removed from any solid bodies, then there will be no preferred directions and no substantial gradients in the statistically-averaged properties of the turbulent velocity field. This suggests that the turbulence will be stationary and isotropic. We shall now derive a semi-quantitative description of some of the statistical properties of such stationary, isotropic turbulence. Our derivation will be based on the following simple physical model:

We shall idealize the turbulent velocity field as made of a set of large eddies, each of which contains a set of smaller eddies and so on. We suppose that each eddy splits into eddies roughly half its size after a few turnover times. This can be described mathematically as nonlinear or triple velocity correlation terms producing, in the law of energy conservation, an energy transfer (a "cascade" of energy) from larger scale eddies to smaller scale eddies. Now, for large enough eddies, we can ignore the effects of genuine viscosity in the flow. However, for small enough eddy scales, viscous dissipation will convert the eddy bulk kinetic energy into heat. This simple model will enable us to derive a remarkably successful formula (the "Kolmogorov spectrum") for the distribution of turbulent energy over eddy size.

We must first introduce and define the turbulent energy per unit wave number and per unit mass, $u_k(k)$. Consider the Fourier transform $\delta\tilde{\mathbf{v}}(\mathbf{k})$ of the fluctuating part of the velocity field $\delta\mathbf{v}(\mathbf{x})$:

$$\boxed{\delta\mathbf{v} = \int \frac{d^3k}{(2\pi)^3}\delta\tilde{\mathbf{v}}e^{i\mathbf{k}\cdot\mathbf{x}}\ .} \tag{15.14}$$

We perform this Fourier transform in much the same way that we take the Fourier transform of the wave function $\psi$ in quantum mechanics: we introduce an imaginary, cubical "box" of volume $\mathcal{V}$ and side $\mathcal{V}^{1/3}$ in which to compute the transform, we require that $\mathcal{V}$ be much larger than the volumes of the largest turbulent eddies, and we treat $\delta\mathbf{v}$ mathematically as though it vanished outside the box's walls. We then define the total energy per unit mass $u$ in the turbulence by

$$\begin{aligned} u = \int \frac{d^3x}{\mathcal{V}}\frac{1}{2}\overline{|\delta\mathbf{v}|^2} &= \int \frac{d^3k}{(2\pi)^3}\frac{\overline{|\delta\tilde{\mathbf{v}}|^2}}{2\mathcal{V}} \\ &= \int_0^\infty dk\, u_k(k)\ , \end{aligned} \tag{15.15}$$

where we have used Parseval's theorem in the second equality, we have used $d^3k = 4\pi k^2 dk$, and we have defined

$$u_k(k) \equiv \frac{\overline{|\delta\tilde{\mathbf{v}}|^2}k^2}{4\pi^2\mathcal{V}}. \tag{15.16}$$

Here the bars denote a time average, $k$ is the magnitude of the wave vector $k \equiv |\mathbf{k}|$ (i.e. it is the wave number or equivalently $2\pi$ divided by the wavelength), and $u_k(k)$ is the *spectral*

*energy per unit mass* of the turbulent velocity field $\delta\mathbf{v}$. In the third equality in Eq. (15.15), we have assumed that the turbulence is isotropic so the integrand depends only on wave number $k$ and not on the direction of $\mathbf{k}$. Correspondingly, we have defined $u_k(k)$ as the energy per unit wave number rather than an energy per unit volume of $\mathbf{k}$-space. Therefore, $u_k(k)dk$ is the average kinetic energy per unit mass associated with modes that have $k$ lying in the interval $dk$; we treat $k$ as positive.

In Chap. 5 we introduced the concept of a "random process" and its "spectral density." The Cartesian components of the fluctuating velocity $\delta v_x$, $\delta v_y$, $\delta v_z$ obviously are random processes, and it is straightforward to show that their spectral densities are related to $u_k(k)$ by

$$\boxed{S_{v_x}(k) = S_{v_y}(k) = S_{v_z}(k) = \text{const} \times u_k(k),} \tag{15.17}$$

where the constant is of order unity.

We shall now use our physical model of turbulence to derive an expression for $u_k(k)$. Denote by $k_{\rm min} = 2\pi/\ell$ the wave number of the largest eddies, and by $k_{\rm max}$ that of the smallest ones (those in which viscosity dissipates the cascading, turbulent energy). Our derivation will be valid, and the result will be valid, only when $k_{\rm max}/k_{\rm min} \gg 1$, i.e. only when there is a large sequence of eddies from the largest to half the largest to a quarter the largest ... down to the smallest.

As a tool in computing $u_k(k)$, we introduce the root-mean-square turbulent turnover speed of the eddies with wave number $k$, $v(k) \equiv v$; and ignoring factors of order unity, we treat the size of these eddies as $k^{-1}$. Then their turnover time is $\tau(k) \sim k^{-1}/v(k) = 1/[kv(k)]$. Our model presumes that in this same time $\tau$ (to within a factor of order unity), each eddy of size $k^{-1}$ splits into eddies of half this size; i.e. the turbulent energy cascades from $k$ to $2k$. Since the energy cascade is presumed stationary (i.e. no energy is accumulating at any wave number), the energy per unit mass that cascades in a unit time from $k$ to $2k$ must be independent of $k$. Denote by $q$ that $k$-independent, cascading energy per unit mass per unit time. Since the energy per unit mass in the eddies of size $k^{-1}$ is $v^2$ (aside from a factor 2, which we neglect), and the cascade time is $\tau \sim 1/(kv)$, then $q \sim v^2/\tau \sim v^3 k$. This tells us that the rms turbulent velocity is

$$v(k) \sim (q/k)^{1/3}. \tag{15.18}$$

Our model lumps together all eddies with wave number within a range $\Delta k \sim k$ around $k$, and treats them all as having wave number $k$. The total energy per unit mass in these eddies is $u_k(k)\Delta k \sim k u_k(k)$ when expressed in terms of the sophisticated quantity $u_k(k)$, and it is $\sim v(k)^2$ when expressed in terms of our simple model. Thus, our model predicts that $u_k(k) \sim v(k)^2/k$, which by Eq. (15.18) implies

$$\boxed{u_k(k) \sim q^{2/3} k^{-5/3} \ \text{ for } k_{\rm min} \ll k \ll k_{\rm max};} \tag{15.19}$$

see Fig. 15.5. This is the *Kolmogorov spectrum* for the spectral energy density of stationary, isotropic, incompressible turbulence. It is valid only in the range $k_{\rm min} \ll k \ll k_{\rm max}$ because only in this range are the turbulent eddies continuously receiving energy from larger length-scales and passing it on to smaller scales. At the ends of the range, the spectrum will be modified in the manner illustrated qualitatively in Fig. 15.5.

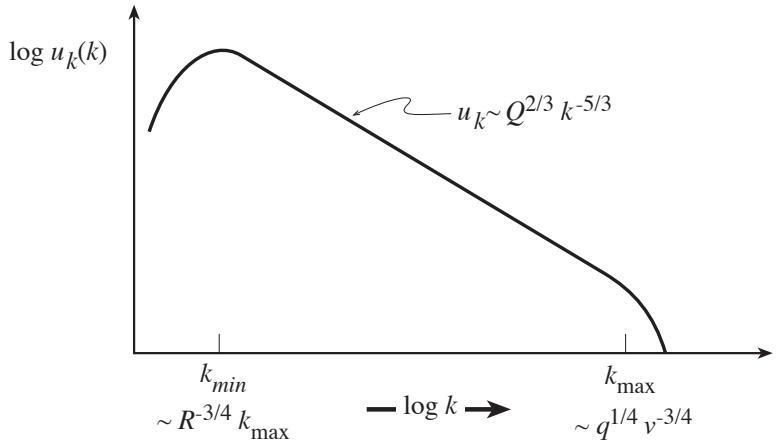


**Fig. 15.5:** The Kolmogorov spectral energy density for stationary, homogeneous turbulence.

The smallest lengthscales present, $k_{\max}^{-1}$, are determined by the fact that there viscous forces become competitive with inertial forces in the Navier-Stokes equation, and thereby convert the cascading energy into heat. Since the ratio of inertial forces to viscous forces is the Reynolds number, the smallest eddies have a Reynolds number of order unity: $R_{k_{\max}} = v(k_{\max})k_{\max}^{-1}/\nu \sim 1$. Inserting Eq. (15.18) for $v(k)$, we obtain

$$k_{\max} \sim q^{1/4}\nu^{-3/4}. \tag{15.20}$$

The largest eddies have sizes $\ell \sim k_{\min}^{-1}$ and turnover speeds $v_\ell = v(k_{\min}) \sim (q/k_{\min})^{1/3}$. By combining these relations with Eq. (15.20) we see that the ratio of the largest wave numbers present in the turbulence to the smallest is

$$\boxed{\frac{k_{\max}}{k_{\min}} \sim \left(\frac{v_\ell \ell}{\nu}\right)^{3/4} = R_\ell^{3/4}.} \tag{15.21}$$

Here $R_\ell$ is the Reynolds number for the flow's largest eddies.

Let us now take stock of our results: If we know the scale $\ell$ of the largest eddies and their rms turnover speeds $v_\ell$ (and, of course, the viscosity of the fluid), then from these we can compute their Reynolds number $R_\ell$; from that, Eq. (15.21), and $k_{\min} \sim \ell^{-1}$, we can compute the flow's maximum and minimum wave numbers; and from $q \sim v_\ell^3/\ell$ and Eq. (15.19) we can compute the spectral energy density in the turbulence.

We can also compute the total time required for energy to cascade from the largest eddies to the smallest: Since $\tau(k) \sim 1/(kv) \sim 1/(q^{1/3}k^{2/3})$, each successive set of eddies feeds its energy downward in a time $2^{-2/3}$ shorter than the preceeding set. As a result, it takes roughly the same amount of time for energy to pass from the second largest eddies (size $\ell/2$) to the very smallest (size $k_{\max}^{-1}$) as it takes for the second largest to extract the energy from the very largest. The total cascade occurs in a time of several $\ell/v_\ell$ (during which time, of course, the mean flow has fed new energy into the largest eddies and they are sending it on downwards).

These results are accurate only to within factors of order unity – with one major exception: The $-5/3$ power law in the Kolmogorov spectrum is very accurate. That this ought to be so one can verify in two equivalent ways: (i) Repeat the above derivation inserting arbitrary factors of order unity at every step. These factors will influence the final multiplicative factor in the Kolmogorov spectrum, but will not influence the $-5/3$ power. (ii) Notice that the only dimensioned entitities that can influence the spectrum in the region $k_{\rm min} \ll k \ll k_{\rm max}$ are the energy cascade rate $q$ and the wave number $k$. Then notice that the only quantity with the dimensions of $u_k(k)$ (energy per unit mass per unit wave number) that can be constructed from $q$ and $k$ is $q^{2/3}k^{-5/3}$. Thus, aside from a multiplicative factor of order unity, this must be the form of $u_k(k)$.

Let us now review and critique the assumptions that went into our derivation of the Kolmogorov spectrum. First, we assumed that the turbulence is stationary and homogeneous. Real turbulence is neither of these, since it exhibits intermittency (Sec. 15.1) and smaller eddies tend to occupy less volume overall than larger eddies. Second, we assumed that the energy source is large-length-scale motion and that the energy transport is local in $k$-space from the large length scales to steadily smaller ones. In the language of a Fourier decomposition into normal modes, we assumed that nonlinear coupling between modes with wave number $k$ causes modes with wave number of order $2k$ to grow, but does not significiantly enhance modes with wave number $100k$ or $0.01k$. Again this is not completely in accord with observations which reveal the development of *coherent structure*–large scale regions with correlated vorticity in the flow. These structures are evidence for a reversed flow of energy in $k$-space from small scales to large scales, and they play a major role in another feature of real turbulence, *entrainment* – the spreading of an organised motion, e.g. a jet, into the surrounding fluid (Ex. 15.6).

Despite these qualifications, the Kolmogorov law is surprisingly useful. It has been verified in many laboratory flows, and it describes many naturally occuring instances of turbulence. For example, the twinkling of starlight is caused by refractive index fluctuations in the earth's atmosphere, whose power spectrum we can determine optically. The underlying turbulence spectrum turns out to be of Kolmogorov form.

**********

## EXERCISES

**Exercise 15.3** *Example: Reynolds Stress, and Fluctuating Part of Navier-Stokes Equation in Weak Turbulence*

(a) Derive the time-averaged Navier-Stokes equation (15.11b) from the time-dependent form of the equation, (15.9b), and thereby infer the definition (15.11c) for the Reynolds stress. Equation (15.11b) shows how the Reynolds stress affects the evolution of the mean velocity. However, it does not tell us how the Reynolds stress evolves.

(b) Explain why an equation for the evolution of the Reynolds stress must involve averages of triple products of the velocity fluctuation. Similarly the time evolution of the averaged triple products will involve averaged quartic products, and so on (cf. the

BBGYK hierarchy of equations in plasma physics, Sec. 21.6). How do you think you might "close" this sequence of equations, i.e. terminate it at some low order and get a fully determined system of equations? [Hint: the simplest way is via the turbulent viscosity.]

(c) Show that the fluctuating part of the Navier-Stokes equation (the difference between the exact Navier-Stokes equation and its time average) takes the following form:

$$\boxed{\frac{\partial \delta\mathbf{v}}{\partial t} + (\bar{\mathbf{v}}\cdot\boldsymbol{\nabla})\delta\mathbf{v} + (\delta\mathbf{v}\cdot\boldsymbol{\nabla})\bar{\mathbf{v}} + [(\delta\mathbf{v}\cdot\boldsymbol{\nabla})\delta\mathbf{v} - \overline{(\delta\mathbf{v}\cdot\boldsymbol{\nabla})\delta\mathbf{v}}] = -\frac{1}{\rho}\boldsymbol{\nabla}\delta P + \nu\nabla^2(\delta\mathbf{v}).} \tag{15.22a}$$

This equation and the fluctuating part of the incompressibility equation

$$\boxed{\boldsymbol{\nabla}\cdot\delta\mathbf{v} = 0} \tag{15.22b}$$

govern the evolution of the fluctuating variables $\delta\mathbf{v}$ and $\delta P$. [The challenge, of course, is to devise ways to solve these equations despite the nonlinearities and the coupling to the mean flow that show up strongly in Eq. (15.22a).]

(d) By dotting $\delta\mathbf{v}$ into Eq. (15.22a) and then taking its time average, derive the following law for the spatial evolution of the turbulent energy density $\frac{1}{2}\rho\overline{\delta v^2}$:

$$\boxed{\bar{\mathbf{v}}\cdot\boldsymbol{\nabla}(\frac{1}{2}\rho\overline{\delta v^2}) + \boldsymbol{\nabla}\cdot\overline{\left(\frac{1}{2}\rho\delta v^2\delta\mathbf{v} + \delta P\delta\mathbf{v}\right)} = -T_R^{ij}\bar{v}_{i,j} + \nu\rho\overline{\delta\mathbf{v}\cdot(\nabla^2\delta\mathbf{v})}\,.} \tag{15.23}$$

Here $T_R^{ij} = \rho\overline{\delta v_i \delta v_j}$ is the Reynolds stress [Eq. (15.11c)]. Interpret each term in this equation.

(e) Now derive a similar law for the spatial evolution of the energy density of ordered motion $\frac{1}{2}\rho\bar{\mathbf{v}}^2$. Show that the energy lost by the ordered motion is compensated by the energy gained by the turbulent energy.

**Exercise 15.4** *Example: Turbulent Wake*
Consider a turbulent wake formed by high Reynolds number flow past a cylinder, as in Ex. 15.1. Let the width a distance $x$ downstream be $w(x)$, the flow speed far upstream be $V$, and the velocity deficit in the mean velocity field of the wake be $\Delta\bar{v}$.

(a) Argue that the kinematic turbulent viscosity in the wake should be $\nu_t \sim \Delta\bar{v}w$. Hence, using a similar order of magnitude analysis to that given in Ex. 15.1, show that the width of the wake is $w \sim (xd)^{1/2}$, where $d$ is the cylinder diameter, and that the velocity deficit is $\Delta\bar{v} \sim V(d/x)^{1/2}$.

(b) Repeat this exercise for a sphere.

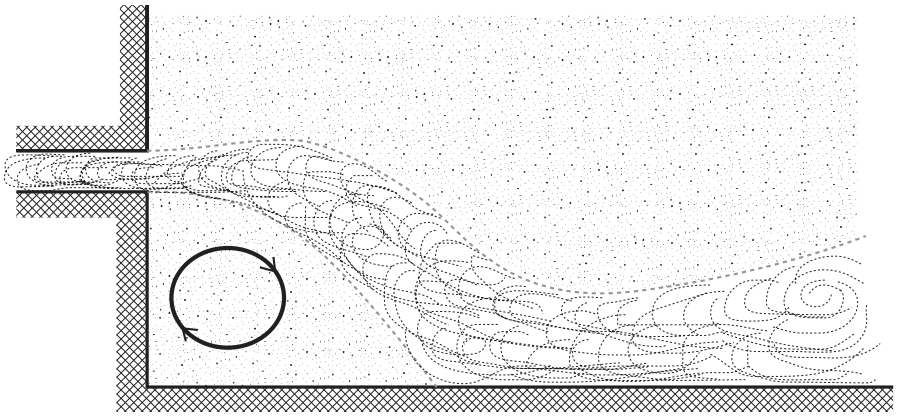

**Fig. 15.6:** The Coanda effect. A turbulent jet emerging from an orfice in the left wall is attracted by the solid bottom wall.

**Exercise 15.5** *Problem: Turbulent Jet*
Now consider a two-dimensional, turbulent jet emerging into an ambient fluid at rest, and contrast it to the laminar jet analyzed in Ex. 15.2.

(a) Find how the velocity and jet width scale with distance downstream from the nozzle.

(b) Repeat the exercise for a three-dimensional jet.

**Exercise 15.6** *Problem: Entrainment and the Coanda Effect*

(a) Evaluate the scaling of the rate of mass flow (discharge) $\dot{M}(x)$ along the three-dimensional, turbulent jet of the previous exercise. Show that it must increase with distance from the nozzle so that mass must be entrained into the flow and become turbulent.

(b) Entrainment is responsible for the *Coanda effect* in which a turbulent jet is attracted by a solid surface (Fig. 15.6). Can you offer a physical explanation for this effect?

(c) Compare the entrainment rate for a turbulent jet with that for a laminar jet (Ex. 15.2). Do you expect the Coanda effect to be larger for a turbulent or a laminar jet?

The Coanda effect is important in aeronautics; for example, it is exploited to prevent the separation of the boundary layer from the upper surface of a wing, thereby improving the wing's lift and reducing its drag.

**Exercise 15.7** *Example: Excitation of Earth's Normal Modes by Atmospheric Turbulence*[3]

[3]Problem devised by David Stevenson; based in part on Tanimoto and Um (1999) who, however, use the pressure spectrum deduced in part (i) rather than the more nearly correct spectrum of part (ii). The difference in spectra does not much affect their conclusions

The Earth has normal modes of oscillation, many of which are in the milliHertz frequency range. Large earthquakes occasionally excite these modes strongly, but the quakes are usually widely spaced in time compared to the ringdown time of a particular mode (typically a few days). There is evidence of a background level of continuous excitation of these modes, with an rms ground acceleration per mode $\sim 10^{-10}$ cm/s$^2$ at seismically "quiet" times. Stochastic forcing by the pressure fluctuations associated with atmospheric turbulence is suspected. This exercise deals with some aspects of this hypothesis.

(a) Estimate the rms pressure fluctuations $P(f)$ at frequency $f$, in a bandwidth equal to frequency $\Delta f = f$, produced on the earth's surface by atmospheric turbulence, assuming a Kolmogorov spectrum for the turbulent velocities and energy. Make your estimate in two ways: (a) via dimensional analysis (what quantity can you construct from the energy cascade rate $q$, atmospheric density $\rho$ and frequency $f$ that has dimensions of pressure?), and (b) via the kinds of arguments about eddy sizes and speeds developed in Sec. 15.3.4.

(b) Your answer in part (i) should scale with frequency as $P(f) \propto 1/f$. In actuality, the measured pressure spectra have a scaling law more nearly like $P(f) \propto 1/f^{2/3}$, not $P(f) \propto 1/f$ [e.g., Fig. 2a of Tanimoto and Um (1999)]. Explain this; i.e., what is wrong with the argument in (i), and how can you correct it to give $P(f) \propto 1/f^{2/3}$? Hint: There is a poem by Lewis Fry Richardson, which says:

> Big whirls have little whirls,
> which feed on their velocity.
> Little whirls have lesser whirls,
> and so on to viscosity.

(c) The low-frequency cutoff for this pressure spectrum is about 0.5 mHz, and at 1 mHz, $P(f)$ has the value $P(f = 1\text{mHz}) \sim 0.3\text{Pa}$, which is about $3 \times 10^{-6}$ of atmospheric pressure. Assuming that 0.5 mHz corresponds to the largest eddies, which have a length scale of a few km (a little less than the scale height of the atmosphere), derive an estimate for the eddies' turbulent viscosity $\nu_t$ in the lower atmosphere. By how many orders of magnitude does this exceed the molecular viscosity? What fraction of the sun's energy input to Earth ($\sim 10^6$ erg cm$^{-2}$ s$^{-1}$) goes into maintaining this turbulence (assumed to be distributed over the lowermost 10 km of the atmosphere)?

(d) At $f = 1$ mHz, what is the characteristic spatial scale (wavelength) of the relevant normal modes of the Earth? [Hint: The relevant modes have few or no nodes in the radial direction. All you need to answer this is a typical wave speed for seismic shear waves, which you can take to be 5 km/s.] What is the characteristic spatial scale (eddy size) of the atmospheric pressure fluctuations at this same frequency, assuming isotropic turbulence? Suggest a plausible estimate for the rms amplitude of the pressure fluctuation averaged over a surface area equal to one square wavelength of the earth's normal modes. (You must keep in mind the random spatially and temporally fluctuating character of the turbulence.)

(e) Using your answer from (iv) and a characteristic shear and bulk modulus for the Earth's deformation of $K \sim \mu \sim 10^{12}$ dyne cm$^{-2}$, comment on how the observed rms normal-mode acceleration ($10^{-10}$ cm s$^{-2}$) compares with that expected from stochastic forcing due to atmospheric turbulence. You may need to go back to Chaps. 10 and 11, and think about the relationship between surface force and surface deformation. [Note: There are several issues in doing this assessment accurately that have not been dealt with in this exercise, e.g. number of modes in a given frequency range; so don't expect to be able to get an answer more accurate than an order of magnitude.]

**********

## 15.4 Turbulent Boundary Layers

Much interest surrounds the projection of spheres of cork, rubber, leather and string by various parts of the human anatomy, with and without the mechanical advantage of levers of willow, ceramic and the finest Kentucky ash. As is well-known, changing the surface texture, orientation, and spin of a ball in various sports can influence the trajectory markedly. Much study has been made of ways to do this both legally and illegally. Some procedures used by professional athletes are pure superstition, but many others find physical explanations that are good examples of the behavior of boundary layers. Many sports involve the motion of balls where the boundary layers can be either laminar or turbulent, and this allows opportunities for controlling the flow. With the goal of studying this, let us now consider the structure of a turbulent boundary layer—first along a straight wall, and later along a ball's surface.

### 15.4.1 Profile of a Turbulent Boundary Layer

In Chap. 13, we derived the Blasius profile for a laminar boundary layer and showed that its thickness a distance $x$ downstream from the start of the boundary layer was roughly $3\delta = 3(\nu x/V)^{1/2}$, where $V$ is the free stream speed; cf. Fig. 13.9. As we have described, when the Reynolds number is large enough, $R_d = Vd/\nu \sim 3 \times 10^5$ or $R_\delta \sim \sqrt{R_d} \sim 500$ in the case of flow past a cylinder (Figs. 15.1 and 15.2), the boundary layer becomes turbulent.

A turbulent boundary layer consists of a thin *laminar sublayer* of thickness $\delta_{\rm ls}$ close to the wall and a much thicker turbulent zone of thickness $\delta_t$; Fig. 15.7. In the following paragraphs we shall use the turbulence concepts developed above to compute, in order of magnitude, the structure of the laminar sublayer and the turbulent zone, and the manner in which those structures evolve along the boundary. We denote by $y$ distance perpendicular to the boundary, and by $x$ distance along it in the direction of the flow.

One key to the structure of the boundary layer is the fact that, in the $x$ component of the time-averaged Navier-Stokes equation, the stress-divergence term $T_{xy,y}$ has the *potential* to be so huge (because of the boundary layer's small thickness) that no other term can compensate it. This is true in the turbulent zone, where $T_{xy}$ is the huge Reynolds stress, and also true in the laminar sublayer, where $T_{xy}$ is the huge viscous stress produced by a huge

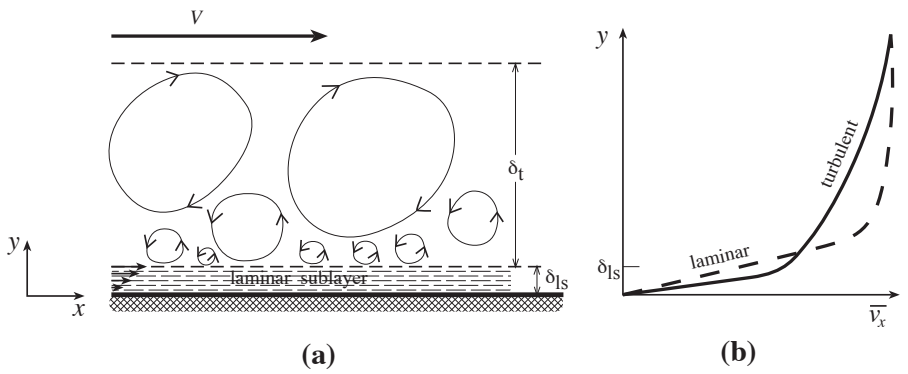


**Fig. 15.7:** Structure of a turbulent boundary layer.

shear that results from the thinness of the layer. (One can check at the end of the following analysis that, for the computed boundary-layer structure, other terms in the $x$ component of the Navier-Stokes equation are indeed so small that they could not compensate a significantly nonzero $T_{xy,y}$.) This *potential* dominance of $T_{xy,y}$ implies that the flow must adjust itself so as to make $T_{xy,y}$ be nearly zero, i.e. $T_{xy}$ be (very nearly) independent of distance $y$ from the boundary.

In the turbulent zone $T_{xy}$ is the Reynolds stress, $\rho v_\ell^2$, where $v_\ell$ is the turbulent velocity of the largest eddies at a distance $y$ from the wall; and therefore constancy of $T_{xy}$ implies constancy of $v_\ell$. The largest eddies at $y$ will have a size $\ell$ of order the distance $y$ from the wall, and correspondingly, the turbulent viscosity will be $\nu_t \sim v_\ell y/3$. Equating the expression $\rho v_\ell^2$ for the Reynolds stress to the alternative expression $2\rho\nu_t \frac{1}{2}\bar{v}_{,y}$ (where $\bar{v}$ is the mean flow speed at $y$ and $\frac{1}{2}\bar{v}_{,y}$ is the shear), and using $\nu_t \sim v_\ell y/3$ for the turbulent viscosity, we discover that in the turbulent zone the mean flow speed varies logarithmically with distance from the wall: $\bar{v} \sim v_\ell \ln y + \text{constant}$. Since the turbulence is created at the inner edge of the turbulent zone, $y \sim \delta_{\rm ls}$, by interaction of the mean flow with the laminar sublayer, the largest turbulent eddies there must have their turnover speeds $v_\ell$ equal to the mean-flow speed there: $\bar{v} \sim v_\ell$ at $y \sim \delta_{\rm ls}$. This tells us the normalization of the logarithmically varying mean flow speed:

$$\boxed{\bar{v} \sim v_\ell[1 + \ln(y/\delta_{\rm ls})] \quad \text{at } y \gtrsim \delta_{\rm ls}.} \tag{15.24}$$

Turn, next to the structure of the laminar sublayer. There the constant shear stress is viscous, $T_{xy} = \rho\nu\bar{v}_{,y}$. Stress balance at the interface between the laminar sublayer and the turbulent zone requires that this viscous stress be equal to the turbulent zone's $\rho v_\ell^2$. This equality implies a linear profile for the mean flow velocity in the laminar sublayer, $\bar{v} = (v_\ell^2/\nu)y$. The thickness of the sublayer is then fixed by continuity of $\bar{v}$ at its outer edge, $(v_\ell^2/\nu)\delta_\ell = v_\ell$. Combining these last two relations, we obtain the following profile and laminar-sublayer thickness:

$$\boxed{\bar{v} \sim v_\ell \left(\frac{y}{\delta_{\rm ls}}\right) \quad \text{at } y \lesssim \delta_{\rm ls} \sim \nu/v_\ell.} \tag{15.25}$$

Having deduced the internal structure of the boundary layer, we turn to the issue of what determines the $y$-independent turbulent velocity $v_\ell$ of the largest eddies. This $v_\ell$ is fixed by

matching the turbulent zone to the free-streaming region outside it. The free-stream velocity $V$ must be equal to the mean flow velocity $\bar{v}$ [Eq. (15.24)] at the outer edge of the turbulent zone. The logarithmic term will dominate, so $V = v_\ell \ln(\delta_t/\delta_{\rm ls})$. Introducing an overall Reynolds number for the boundary layer,

$$R_\delta \equiv V\delta_t/\nu, \tag{15.26}$$

and noting that turbulence requires a huge value ($\gtrsim 1000$) of this $R_\delta$, we can reexpress $V$ as $V \sim v_\ell \ln R_\delta$. This should actually be regarded as an equation for the turbulent velocity of the largest scale eddies in terms of the free-stream velocity:

$$\boxed{v_\ell \sim \frac{V}{\ln R_\delta}.} \tag{15.27}$$

If the thickness $\delta_t$ of the entire boundary layer and the free-stream velocity $V$ are given, then Eq. (15.26) determines the boundary layer's Reynolds number, Eq. (15.27) then determines the turbulent velocity, and Eqs. (15.25) and (15.24) determine the layer's internal structure.

Turn, finally, to the issue of how the boundary layer thickness $\delta_t$ evolves with distance $x$ down the wall (and correspondingly, how all the rest of the boundary layer's structure, which is fixed by $\delta_t$, evolves). At the turbulent zone's outer edge, the largest turbulent eddies move with speed $v_\ell$ into the free-streaming fluid, entraining that fluid into themselves (cf. Ex. 15.6 on entrainment and the Coanda effect). Correspondingly, the thickness grows at a rate

$$\boxed{\frac{d\delta_t}{dx} = \frac{v_\ell}{V} = \frac{1}{\ln R_\delta}\,.} \tag{15.28}$$

Since $\ln R_\delta$ depends only extremely weakly on $\delta_t$, *the turbulent boundary layer expands essentially linearly with distance $x$, by contrast with a laminar boundary layer's $\delta \propto x^{1/2}$.*

One can easily verify that, not only does the turbulent boundary layer expand more rapidly than the corresponding laminar boundary layer would, if it were stable, but the turbulent layer is also thicker at all locations down the wall. Physically, this can be traced to the fact that the turbulent boundary layer involves a three-dimensional velocity field, whereas the corresponding laminar layer would involve only a two-dimensional field. The enhanced thickness and expansion contribute to an enhanced ability to withstand an adverse pressure gradient and to cling to the surface without separation (the "Coanda effect"; Fig. 15.6 and Ex. 15.6).

However, there is a price to be paid for this benefit. Since the velocity gradient is increased close to the surface, the actual surface shear stress exerted by the turbulent layer, through its laminar sublayer, is significantly larger than in the corresponding laminar boundary layer. As a result, if the layer were to remain laminar, that portion that would adhere to the surface would produce less viscous drag than the corresponding portion of the turbulent layer. Correspondingly, in a long, straight pipe, the drag on the pipe wall goes up when the boundary layer becomes turbulent.

However, for flow around a cylinder or other confined body, the drag goes down! cf. Fig. 15.2. The reason is that in the separated, laminar boundary layer the dominant source

of drag is not viscosity but rather a pressure differential between the front face of the cylinder, where the layer adheres, and the back face where the reverse eddies circulate. The pressure is much lower in the back-face eddies than in the front-face boundary layer, and that pressure differential gives rise to a significant drag, which gets reduced when the layer goes turbulent and adheres to the back face. Therefore, if one's goal is to reduce the overall drag and the laminar flow is prone to separation, a nonseparating (or delayed-separation) turbulent layer is to be prefered over the laminar layer. Similarly (and for essentially the same reason), for an airplane wing, if one's goal is to maintain a large lift, then a nonseparating (or delayed-separation) turbulent layer is to be prefered over a separating, laminar one.[4]

For this reason, steps are often taken in engineering flows to ensure that boundary layers become and remain turbulent. A crude but effective example is provided by the vortex generators that are installed on the upper surfaces of some airfoils. These are small obstacles on the wing which penetrate through a laminar boundary layer into the free flow. By changing the pressure distribution, they force air into the boundary layer and initiate three-dimensional vortical motion in the boundary layer forcing it to become partially turbulent. This allows airplanes to climb more steeply without stalling due to boundary-layer separation, and it helps reduce aerodynamical drag.

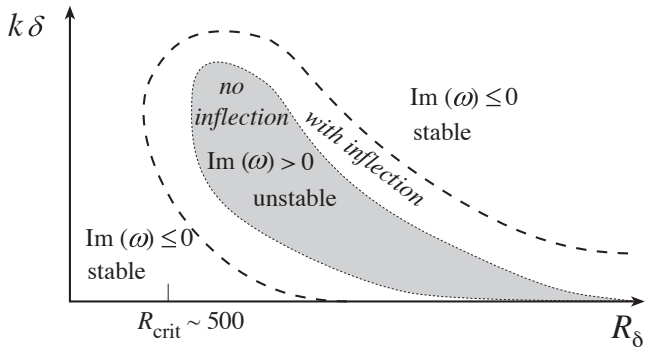


**Fig. 15.8:** Values of wave number $k$ for stable and unstable wave modes in a laminar boundary layer with thickness $\delta$, as a function of the boundary layer's Reynolds number $R_\delta = V\delta/\nu$. If the unperturbed velocity distribution $v_x(y)$ has no inflection point, i.e. if $d^2v_x/dy^2 < 0$ everywhere as is the case for the Blasius profile (Fig. 13.9), then the unstable modes are confined to the shaded region. If there is an inflection point (so $d^2v_x/dy^2 > 0$ near the wall but becomes negative farther from the wall), as is the case near a surface of separation (Fig. 13.11), then the unstable region is larger and does not asymptote to $k = 0$ as $R_\delta \to \infty$, i.e. it has a boundary like the dashed curve.

### 15.4.2 Instability of a Laminar Boundary Layer

Much work has been done on the linear stability of laminar boundary layers. The principles of such stability analyses should now be familiar, although the technical details are formidable.

[4]Another example of separation occurs in "Lee waves" which can form when wind blows over a mountain range. These consist of standing-wave eddies in the separated boundary layer, somewhat analogous to the Karman vortex street of Fig. 15.2(d); and they are sometimes used by glider pilots to regain altitude.

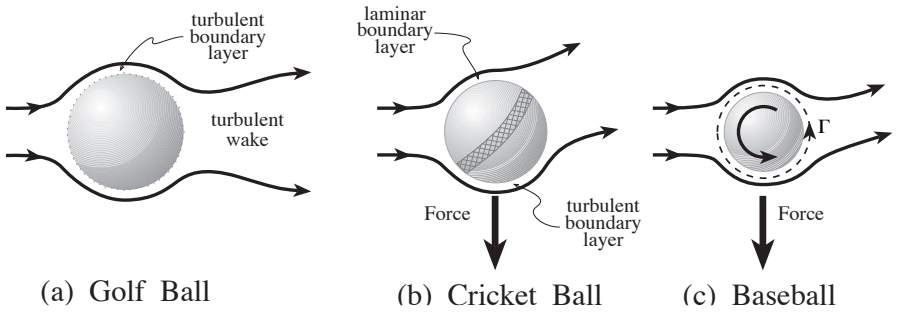


**Fig. 15.9:** Boundary layers around golf balls, cricket balls, and baseballs, as they move leftward relative to the air — i.e., as the air flows rightward as seen in their rest frames.

In the simplest case an equilibrium flow like the Blasius profile is identified and the equations governing the time evolution of small perturbations are written down. The spatial and temporal evolution of individual Fourier components is assumed to vary as $\exp i(\mathbf{k}\cdot\mathbf{x}-\omega t)$, and we seek modes that have zero velocity perturbation on the solid surface past which the fluid flows, and that decay to zero in the free stream. We ask whether there are unstable modes, i.e., modes with real $\mathbf{k}$ for which the imaginary part of $\omega$ is positive so they grow exponentially in time. The results can generally be expressed in the form of a diagram like Fig. 15.8.

It is found that there is generally a critical Reynolds number at which one mode becomes unstable. At higher values of the Reynolds number a range of k-vectors are unstable. One interesting result of these calculations is that in the absence of viscous forces (i.e., in the limit $R_\delta \to \infty$), the boundary layer is unstable if and only if there is a point of inflection in the velocity profile (a point where $d^2v_x/dy^2$ changes sign); cf. Fig. 15.8 and Ex. 15.9.

Although, in the absence of an inflection, an inviscid flow $v_x(y)$ is stable, for some such profiles even the slightest viscosity can trigger instability. Physically, this is because viscosity can tap the relative kinetic energies of adjacent flow lines. Viscous-triggered instabilities of this sort are sometimes called *secular instabilities* by contrast with the *dynamical instabilities* that arise in the absence of viscosity. Secular instabilities are quite common in fluid mechanics.

### 15.4.3 The flight of a ball.

Having developed some insights into boundary layers and their stability, we now apply those insights to the balls used in various sports.

The simplest application is to the dimples on a golf ball [Fig. 15.9(a)]. The dimples provide finite-amplitude disturbances in the flow which can initiate the formation of growing wave modes and turbulence in the boundary layer. The adherence of the boundary layer to the ball is improved and separation occurs further behind the ball leading to a lower drag coefficient and a greater range of flight; see Figs. 15.2 and 15.9(a).

A variant on this mechanism is found in the game of cricket, which is played with a ball whose surface is polished leather with a single equatorial seam of rough stitching. When the ball is "bowled" in a non-spinning way with the seam inclined to the direction of motion,

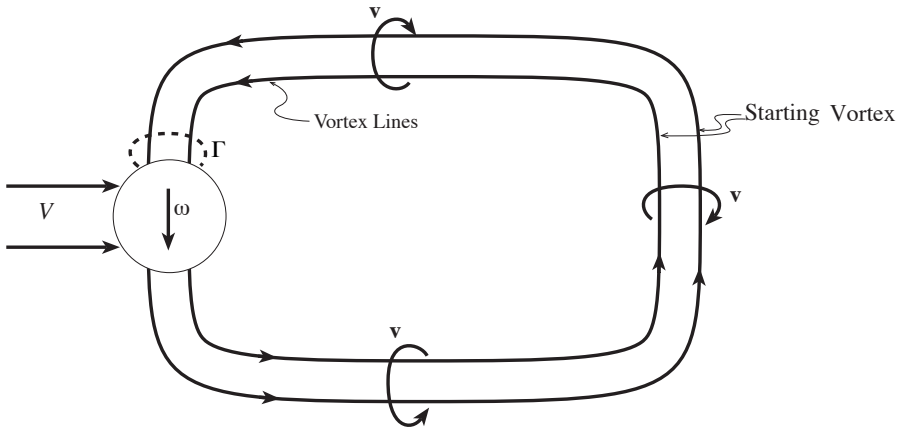


**Fig. 15.10:** Vortex lines passing through a spinning ball. The starting vortex is created and shed when the ball is thrown, and is carried downstream by the flow as seen in the ball's frame of reference. The vortex lines connecting this starting vortex to the ball lengthen as the flow continues.

there is a laminar boundary layer on the smooth side and a turbulent boundary layer on the side with the rough seam [Fig. 15.9(b)]. These two boundary layers separate at different points behind the flow leading to a net deflection of the air. The ball will therefore swerve towards the side with the leading seam. (The effect is strongest when the ball is new and still shiny and on days when the humidity is high so the thread in the seam swells and is more efficient at making turbulence.)

This mechanism is different from that used to throw a slider or curveball in baseball, in which the pitcher causes the ball to spin about an axis roughly perpendicular to the direction of motion. In the slider the axis is vertical; for a curveball it is inclined at about 45° to the vertical. The spin of the ball creates circulation (in a nonrotating, inertial frame) like that around an airfoil. The pressure forces associated with this circulation produce a net sideways force in the direction of the baseball's rotational velocity on its leading hemisphere, i.e. as seen by the hitter [Fig. 15.9(c)]. The physical origin of this effect is actually quite complex and is only properly described with reference to experimental data. The major effect is that separation is delayed on the side of the ball where the rotational velocity is in the same direction as the airflow, and happens sooner on the opposite side [Fig. 15.9(c)], leading to a pressure differential. The reader may be curious as to how this circulation can be established in view of Kelvin's theorem, Eq. (13.15), which tells us that if we use a circuit that is so far from the ball and its wake that viscous forces cannot cause the vorticity to diffuse to it, then the circulation must be zero. What actually happens is that when the flow is initiated, starting vortices are shed by the ball and are then convected downstream, leaving behind the net circulation $\Gamma$ that passes through the ball (Fig. 15.10). This effect is very much larger in two dimensions with a rotating cylinder than in three dimensions because the magnitude of the shed vorticity is much larger. It goes by the name of *Magnus effect* in two dimensions and *Robins effect* in three. It is also useful in understanding the lift in airfoils.

In table tennis, a drive is often hit with *topspin* so that the ball rotates about a horizontal axis perpendicular to the direction of motion. In this case, the net force is downwards and the

ball falls faster toward the ground, the effect being largest after it has somewhat decelerated. This allows a ball to be hit hard over the net and bounce before passing the end of the table, increasing the margin for errors in the direction of the hit.

Those wishing to improve their curveballs or cure a bad slice are referred to the monographs by Adair (1990), Armenti (1992) and Lighthill (1986).

**********

## EXERCISES

**Exercise 15.8** *Problem: Effect of drag*
A well hit golf ball travels about 300 yards. A fast bowler or fastball pitcher throws a ball at over 90 m.p.h (miles per hour). A table tennis player can hit a forehand return at about 30 m.p.h. The masses and sizes of each of these three types of balls are $m_g \sim 46\text{g}, d_g \sim 43\text{mm}, m_c \sim 160\text{g}, d_c \sim 70\text{mm}, m_b \sim 140\text{g}, d_b \sim 75\text{mm}, m_{tt} \sim 2.5\text{g}, d_{tt} \sim 38\text{mm}$.

(a) For golf, cricket (or baseball) and table tennis, estimate the Reynolds number of the flow and infer the drag coefficient, $C_D$. (The variation of $C_D$ with $R_d$ can be assumed to be similar to that in flow past a cylinder.)

(b) Hence estimate the importance of aerodynamic drag in determining the range of a ball in each of these three cases.

**Exercise 15.9** *Problem: Tollmein-Schlicting Waves*
Consider an inviscid ($\nu = 0$), incompressible flow near a plane wall where a boundary layer is established. Introduce coordinates $x$ parallel to the wall and $y$ perpendicular to the wall. Let the components of the equilibrium velocity be $\{v_x(y), v_y(y), 0\}$.

(a) Show that a small perturbation in the velocity, $\delta v_y \propto \exp ik(x - ct)$, with $k$ real and frequency $ck$ possibly complex, satisfies the differential equation

$$\frac{\partial^2 \delta v_y}{\partial y^2} = \left[\frac{1}{(v_x - c)}\frac{d^2 v_x}{dy^2} + k^2\right]\delta v_y \ . \tag{15.29}$$

Hence argue that a sufficient condition for unstable wave modes ($\text{Im}(c) > 0$), is that the velocity field possess a point of inflection; cf. Fig. 15.8. (The boundary layer can also be unstable in the absence of a point of inflection, but viscosity must be present to trigger the instability.)

**********

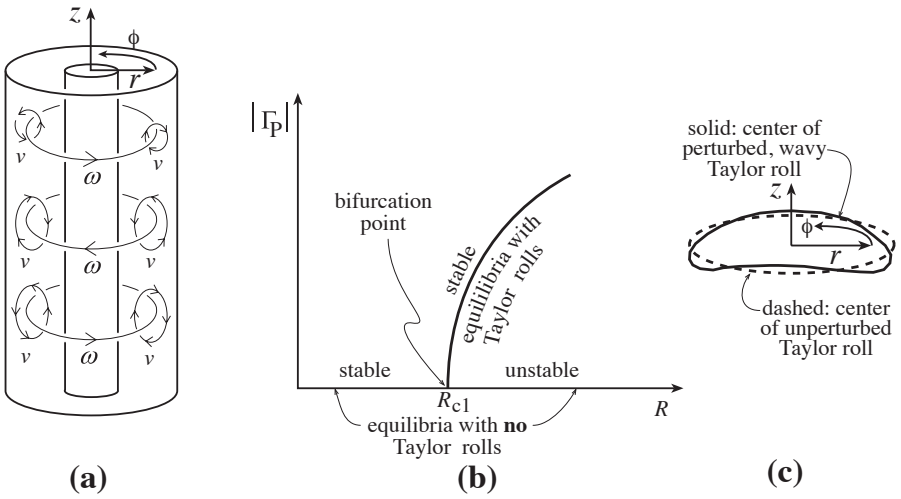


**Fig. 15.11:** Bifurcation in Couette flow. (a) Equilibrium flow with Taylor rolls. (b)Bifurcation diagram in which the amplitude of the poloidal circulation $|\Gamma_{\rm P}|$ in a Taylor roll is plotted against the Reynolds number $R$. At low $R$ ($R < R_{c1}$) the only equilibrium flow configuration is smooth, azimuthal flow. At larger $R$ ($R_{c1} < R < R_{c2}$) there are two equilibria, one with Taylor rolls and stable, the other the smooth, azimuthal flow, which has become unstable. (c) Shape of a Taylor roll at $R_{c1} < R < R_{c2}$ (dashed ellipse) and at higher $R$, $R_{c2} < R < R_{c3}$ (wavy curve).

## 15.5 The Route to Turbulence: Onset of Chaos

### 15.5.1 Couette Flow

Let us examine qualitatively how a viscous flow becomes turbulent. A good example is Couette flow between two long, concentric, relatively rotating cylinders as introduced in Chap. 13 and depicted in Fig. 15.11(a). The Rayleigh stability criterion (flow unstable if and only if angular momentum per unit mass decreases outward) was derived in Chap. 13 ignoring viscous stress. Now suppose we have a flow that is stable according to the Rayleigh criterion. Suppose, further, that the fluid is a liquid and we steadily decrease its viscosity by heating it, so that the Reynolds number steadily increases. At low $R$, the equilibrium flow is stationary and azimuthal [strictly in the $\phi$ direction in Fig. 15.11(a)]. However, at some critical Reynolds number $R_{c1}$, the flow becomes unstable to the growth of small perturbations, and these perturbations drive a transition to a new, stationary equilibrium that involves poloidal circulation (quasi-circular motions in the $r$ and $z$ directions, called *Taylor rolls*); see Fig. 15.11(a).

What has happened is that an equilibrium with a high degree of symmetry has become unstable and a new, lower-symmetry, stable equilibrium has taken over. Translational invariance in the direction of the cylinder axis has been lost from the flow, despite the fact that the boundary conditions remain translationally symmetric. This change of equilibrium mode is another example of a bifurcation like that discussed when we treated the buckling of beams and playing cards (Chaps. 10 and 11).

As $R$ is increased further, this process repeats: At a second critical Reynolds number

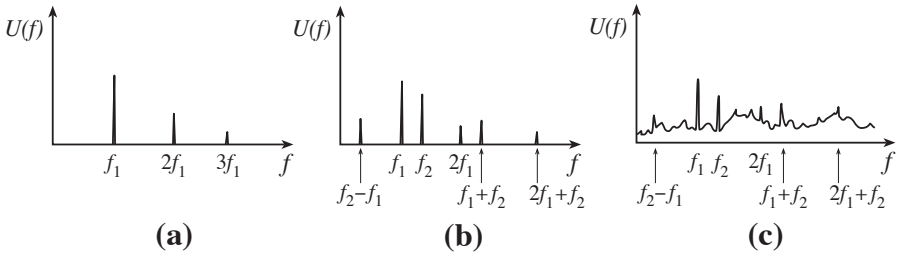


**Fig. 15.12:** The energy spectrum of velocity fluctuations in rotating Couette flow (schematic). (a) For a moderate Reynolds number, $R_{c2} < R < R_{c3}$, at which the stable equilibrium flow is that with the wavy Taylor rolls of Fig. 15.11(c). (b) For a higher Reynolds number, $R_{c3} < R < R_{c4}$, at which the stable flow has wavy Taylor rolls with two incommensurate fundamental frequencies present. (c) For a still higher Reynolds number, $R > R_{c4}$, at which turbulence has set in.

$R_{c2}$ there is a second bifurcation of equilibria in which the azimuthally smooth Taylor rolls become unstable and are replaced by new, azimuthally wavy Taylor rolls; see Fig. 15.11(c). Again, an equilibrium with higher symmetry (rotation invariance) has been replaced, at a bifurcation point, by one of lower symmetry (no rotation invariance). There is a fundamental frequency $f_1$ associated with the wavy Taylor rolls' motion as they circulate around the central cylinder. Since the waves are nonlinearly large, harmonics of this fundamental are also seen when one Fourier decomposes the velocity field; cf. Fig. 15.12(a). When $R$ is increased still further to some third critical value $R_{c3}$, there is yet another bifurcation. The Taylor rolls now develop a second set of waves, superimposed on the first, with a corresponding new fundamental frequency $f_2$ that is incommensurate with $f_1$. In the energy spectrum one now sees various harmonics of $f_1$ and of $f_2$, as well as sums and differences of these two fundamentals; cf. Fig. 15.12(b).

It is exceedingly difficult to construct experimental apparatus that is clean enough, and free enough from the effects of finite lengths of the cylinders, to reveal what happens next as one turns up the Reynolds number. However, despite the absence of clean experiments, it seemed obvious before the 1970's what would happen: The sequence of bifurcations would continue, with ever decreasing intervals of Reynolds number $\Delta R$ between them, producing after awhile such a complex maze of frequencies, harmonics, sums, and differences, as to be interpreted as turbulence. Indeed, one finds the onset of turbulence described in just this manner in the classic fluid mechanics textbook of Landau and Lifshitz (1959).

The 1970's and 1980's brought a major breakthrough in our understanding of the onset of turbulence. This breakthrough came from studies of model dynamical systems with only a few degrees of freedom, in which nonlinear effects play similar roles to the nonlinearities of the Navier-Stokes equation. These studies revealed only a handful of routes to irregular or unpredictable behavior known as chaos, and none were of the Landau-Lifshitz type. However, one of these routes starts out in the same manner as does rotating Couette flow: As a control parameter (Reynolds number for Couette flow) is gradually increased, first oscillations with one fundamental frequency $f_1$ and its harmonics turn on; then a second frequency $f_2$ and its harmonics turn on, along with sums and differences of $f_1$ and $f_2$; and then, suddenly, chaos sets in. Moreover, the chaos is clearly not being produced by a complicated superposition

of other, new frequencies; it is fundamentally different from that. The best Couette-flow experiments of the 1980's and later appear to confirm that the onset of turbulence goes by this route; see Fig. 15.12(c).

### 15.5.2 Feigenbaum Sequence

The very simplest of systems in which one can study the several possible routes to chaos are one-dimensional mathematical maps. A lovely example is the "Feigenbaum sequence," explored by Mitchell Feigenbaum in the 1970's.

The Feigenbaum sequence is a sequence $\{x_1, x_2, x_3, \ldots\}$ of values of a real variable $x$, given by the rule (sometimes called the *logistic equation*) [5]

$$x_{n+1} = 4ax_n(1 - x_n). \tag{15.30}$$

Here $a$ is a fixed "control" parameter. It is easy to compute Feigenbaum sequences $\{x_n\}$ for different values of $a$ on a personal computer (Ex. 15.10). What is found is that there are critical parameters $a_1, a_2, \ldots$ at which the character of the sequence changes sharply. For $a < a_1$, the sequence asymptotes to a stable fixed point. For $a_1 < a < a_2$, the sequence asymptotes to stable, periodic oscillations between two fixed points. If we increase the parameter further, so that $a_2 < a < a_3$, the sequence becomes a periodic oscillation between four fixed points. The period of the oscillation has doubled. This *period doubling* (NOT frequency doubling) happens again: When $a_3 < a < a_4$, $x$ asymptotes to regular motion between eight fixed points. Period doubling increases with shorter and shorter intervals of $a$ until at some value $a_\infty$, the period becomes infinite and the sequence does not repeat. Chaos has set in.

This period doubling is a second route to chaos, very different in character from the "one-frequency, two-frequencies, chaos" route that one meets in Couette flow. Remarkably, fluid dynamical turbulence can set in by this second route, as well as by the first. It does so in certain very clean experiments on convection in liquid helium. We shall return to this below, and then again in Chap. 17.

How can so starkly simple and discrete a thing as a one-dimensional map bear any relationship at all to the continuous solutions of the fluid dynamical differential equations? The answer is quite remarkable:

Consider a steady flow in which one parameter $a$ (e.g. the Reynolds number) can be adjusted. Now, as we change $a$ and approach turbulence, the flow may develop a periodic oscillation with a single frequency $f_1$. We could measure this by inserting some probe at a fixed point in the flow to measure a fluid variable $y$, e.g. one component of the velocity. We can detect the periodicity either by inspecting the readout $y(t)$ or its Fourier transform $\tilde{y}$. However, there is another way, that may be familiar from classical mechanics. This is to regard $\{y, \dot{y}\}$ as the two coordinates of a two-dimensional phase space. (Of course the dimensionality of the phase space could be arbitrarily large, but let us keep matters as simple

[5] This equation first appeared in discussions of population biology (Verhulst, 1838). If we consider $x_n$ as being proportional to the number of animals in a species, the number in the next season should be proportional to the number of animals already present and to the availability of resources which will decrease as $x_n$ approaches some maximum value, in this case unity. Hence the terms $x_n$ and $1 - x_n$ in Eq. (15.30).

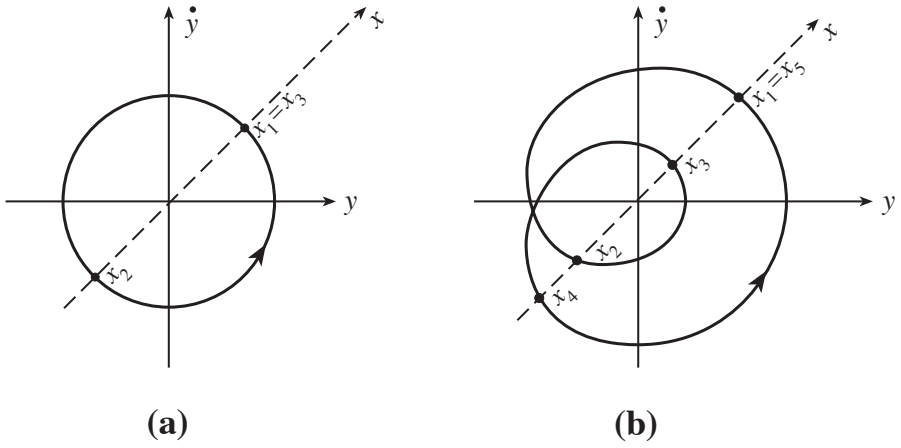


**Fig. 15.13:** a) Representation of a single periodic oscillation as motion in phase space. b) Motion in phase space after period doubling. The behavior of the system may also be described by using the coordinate $x$ of the Poincaré map.

as possible.) For a single periodic oscillation, the system will follow a closed path in this phase space [Fig. 15.13(a)]. As we increase $a$ further, a period doubling may occur and the trajectory in phase space may look like Fig. 15.13(b). Now, as we are primarily interested in the development of the oscillations, we need only keep one number for every fundamental period $P_1 = 1/f_1$. Let us do this by taking a section through phase space and introducing a coordinate $x$ on this section as shown in Fig. 15.13. The $n$'th time the trajectory crosses through this section, its crossing point is $x_n$, and the mapping from $x_n$ to $x_{n+1}$ can be taken as a representative characterization of the flow. When only the frequency $f_1$ is present, the map will read $x_{n+2} = x_n$ [Fig. 15.13(a)]. When $f_1$ and $f_2 = \frac{1}{2}f_1$ are present, the map will read $x_{n+4} = x_n$ [Fig. 15.13(b)]. (These specific maps are overly simple compared to what one may encounter in a real flow, but they illustrate the idea.)

To reiterate, instead of describing the flow by the full solution $\mathbf{v}(\mathbf{x}, t)$ to the Navier-Stokes equations and the flow's boundary conditions, we can construct the simple map $x_n \to x_{n+1}$ to characterize the flow. This procedure is known as a *Poincaré map*. The mountains have labored and brought forth a mouse! However, this mouse turns out to be all that we need. For the convection experiments, just the same period doubling behavior and approach to chaos are present in these maps as in the original phase-space diagram and in the full solution to the fluid dynamical equations; and when observed in the Poincaré maps, it looks qualitatively the same as in the Feigenbaum sequence. It is remarkable that for a system with so many degrees of freedom, chaotic behavior can be observed by suppressing almost all of them.

If, in the period-doubling route to chaos, we compute the limiting ratio,

$$\mathcal{F} = \lim_{j\to\infty} \frac{a_j - a_{j-1}}{a_{j+1} - a_j}, \tag{15.31}$$

we find that it has the value $4.6692016090\ldots$. This (Feigenbaum) number seems to be a universal constant characteristic of most period doubling routes to chaos, independent of the

particular map that was used. For example, if we had used

$$x_{n+1} = a \sin \pi x_n \tag{15.32}$$

we would have got the same constant.

The most famous illustration of the period doubling route to chaos is a classic experiment by Libchaber and Maurer (1978) on convection in liquid helium. The temperature at a point was monitored with time as the helium's vertical temperature gradient was slowly increased. Initially, the temperature was found to oscillate with a single period, but then subharmonics started appearing one after another, until, eventually, the flow became turbulent. Libchaber was able to measure the ratio (15.31) accurate to about 3 per cent (with $a_j$ the temperature at which the $j$'th period doubling occurred). His result agreed with Feigenbaum's number to within his experimental accuracy!

For several other routes to chaos identified in convection experiments, see Gollub and Benson (1980).

When chaos sets in, the evolution of the system becomes essentially incalculable. This is because, as can be shown mathematically, the future state, as measured by the values of a set of fluid variables at some subsequent time (or by the value of a map), becomes highly sensitive to the assumed initial conditions. Paths in phase space (or in the mapping) that start extremely close to one another diverge from each other exponentially rapidly with time.

It is important to distinguish the unpredictability of classical chaos from unpredictability in the evolution of a quantum mechanical system. A classical system evolves under precisely deterministic differential equations. Given a full characterization of the system at any time $t$, the system is fully specified at a time $t + \Delta t$ later for any $\Delta t$. However, what characterizes a chaotic system is that the evolution of two identical systems in neighboring initial states will eventually evolve so that they follow totally different histories. The time for this to happen is called the Lyapunov time (see Ex. 14.11). The practical significance of this essentially mathematical feature is that if, as will always be the case, we can only specify the initial state up to a given accuracy (due to practical considerations, not issues of principle), then the true initial state could be any one of those lying in some region, and we have no way of predicting what the state will be after a few Lyapunov times. Quantum mechanical indeterminacy is different. If we can prepare a system in a given state described by a wave function, the evolution will be governed quite deterministically by the time-dependent Schrödinger equation. However, if we choose to make a measurement of an observable, many quite distinct outcomes are immediately possible and the system will be left in an eigenstate corresponding to the actual measured outcome. The quantum mechanical description of classical chaos is the subject of quantum chaos.

The realisation that many classical systems have an intrinsic unpredictability despite being deterministic from instant to instant has been widely publicised in popularisations of research into chaos. However it is not particularly new. It was well understood, for example, by Poincaré at the turn of the century, and watching the weather report on the nightly news bears witness to its dissemination into the popular culture! What *is* new and intriguing is the manner in which the transition from a deterministic to a non-predictable evolution happens.

Chaotic behavior is well documented in a variety of physical dynamical systems: electrical

circuits, nonlinear pendula, dripping faucets, planetary motions and so on. The extent to which the principles that have been devised to describe chaos in these systems can also be applied to general fluid turbulence remains a matter for debate. There is no question that there are similarities, and there has been quantitative success in applying chaos results to a limited form of turbulent convection. However, most forms of turbulence are not so easily described and there is still a huge gap between the intriguing mathematics of chaotic dynamics and practical applications to natural and technological flows.

**********

## EXERCISES

**Exercise 15.10** *Problem: Feigenbaum Sequence*
Use a computer to calculate the first five critical parameters $a_j$ in the Feigenbaum sequence, Eq. (15.30). Hence verify that the ratio of successive differences, tends toward the limit quoted in Eq. (15.31). (Hint. You might find it helpful to construct a graph to find suitable starting values, $x_1$ and starting parameters $a$.)

**Exercise 15.11** *Example: Lyapunov Exponent*
Consider the logistic equation (15.30) for the special case $a = 1$, which is large enough to ensure that chaos has set in.

(a) Make the substitution $x_n = \sin^2 \pi\theta_n$ and show that the equation can be expressed in the form $\theta_{n+1} = 2\theta_n (\text{mod } 1)$; i.e., $\theta_{n+1} =$ fractional part of $2\theta_n$. .

(b) Write $\theta_n$ as a "binimal" (binary decimal). For example $11/16 = 1/2 + 1/8 + 1/16$ has the binary decimal form 0.1011 . Explain what happens to this number in each successive iteration.

(c) Now suppose that an error is made in the i'th digit of the starting binimal. When will it cause a major error in the predicted value of $x_n$?

(d) If the error after $n$ iterations is written $\epsilon_n$, show that the Lyapunov exponent $p$ defined by

$$p = \lim_{n\to\infty} \frac{1}{n} \ln \left| \frac{\epsilon_n}{\epsilon_0} \right| \tag{15.33}$$

is $\ln 2$ (so $\epsilon_n \simeq 2^n \epsilon_0$ for large enough $n$). Lyapunov exponents play an important role in the theory of dynamical systems.

**Exercise 15.12** *Example: Strange Attractors*
Another interesting one-dimensional map is provided by the recursion relation,

$$x_{n+1} = a \left( 1 - 2 \left| x_n - \frac{1}{2} \right| \right) \tag{15.34}$$

(a) Consider the asymptotic behavior of the variable $x_n$ for different values of the parameter $a$, with both $x_n$ and $a$ being confined to the interval $[0, 1]$. In particular find that for $0 < a < a_{\rm crit}$ (for some $a_{\rm crit}$), the sequence $x_n$ converges to a stable fixed point, but for $a_{\rm crit} < a < 1$, the sequence wanders chaotically through some interval $[x_{\rm min}, x_{\rm max}]$.

(b) Using a computer, calculate the value of $a_{\rm crit}$ and the interval $[x_{\rm min}, x_{\rm max}]$ for $a = 0.8$.

(c) The interval $[x_{\rm min}, x_{\rm max}]$ is an example of a *strange attractor*. It has the property that if we consider sequences with arbitrarily close starting values, their values of $x_n$ in this range will eventually diverge. Show that the attractor is strange by computing the sequences with $a = 0.8$ and starting values $x_1 = 0.5, 0.51, 0.501, 0.5001$. Determine the number of iterations $n_\epsilon$ required to produce significiant divergence as a function of $\epsilon = x_1 - 0.5$. It is claimed that $n_\epsilon \sim -\ln_2(\epsilon)$. Can you verify this? Note that the onset of chaos at $a = a_{\rm crit}$ is quite sudden in this case, unlike the behavior exhibited by the Feigenbaum sequence.

**Exercise 15.13** *Problem: Lorenz equations*
One of the first discoveries of chaos in a mathematical model was by Lorenz (1963), who made a simple model of atmospheric convection. In this model, the temperature and velocity field are characterized by three variables, $x, y, z$, which satisfy the coupled, nonlinear differential equations

$$\begin{aligned} \dot{x} &= 10(y - x) \ , \\ \dot{y} &= -xz + 28x - y \ , \\ \dot{z} &= xy - 8z/3 \ . \end{aligned} \tag{15.35}$$

(The precise definitions of $x, y, z$ need not concern us here.) Integrate these equations numerically to show that $x, y, z$ follow non-repeating orbits in the three-dimensional phase space that they span, but follow certain broadly defined paths in this space. (It may be helpful to plot out the trajectories of pairs of the dependent variables.)
[Note: These Lorenz equations are often studied with the numbers 10, 28, 8/3 replaced by parameters $\sigma$, $\rho$, and $\beta$. As these parameters are varied, the behavior of the system changes.]

**********

# Bibliographic Note

Turbulence is omitted from many standard textbooks on fluid mechanics, aside from brief descriptions, presumably because it is so poorly understood. Good textbook treatments can be found in White (1991), Tennekes and Lumley (1972), and from a more physical perspective, Tritton (1977). To develop physical insight into turbulence, we recommend

**Box 15.2**
**Important Concepts in Chapter 14**

- Weak turbulence contrasted with strong or fully developed turbulence, Sec. 15.1
- Scaling relation, Sec. 15.2
- Stagnation pressure, Sec. 15.2
- Drag coefficient, Sec. 15.2
- Karman vortex street, Sec. 15.2
- Critical Reynolds number, $R_d \sim 1000$, for onset of turbulence, Sec. 15.2
- Entrainment, Coanda effect, and its role on airplane wings, Secs. 15.2, 15.4.1, Ex. 15.6
- Intermittency, Sec. 15.1
- Role of vorticity in turbulence: stretching of vortex tubes, Sec. 15.3.3, Fig. 15.4
- Eddies, energy cascade, viscous damping at smallest scale, Sec. 15.3.4
- Kolmogorov spectrum, Sec. 15.3.4
- Weak turbulence theory, Sec. 15.3
  - Decomposition into time averaged flow and fluctuating flow, Sec. 15.3.1
  - Reynolds stress, tubulent viscosity, and their role in coupling fluctuating flow to time-averaged flow, Secs. 15.3.1, 15.3.2
  - The physics that governs the structure of the time-averaged flow in boundary layers, wakes and jets, Sec. 15.4.1, Exs. 15.4, 15.5
- Secular instability contrasted with dynamical instability, Sec. 15.4.2
- Rotating Couette flow, Sec. 15.5.1
- Poincaré map and its use to produce discrete maps that characterize a flow, Sec. 15.5.2
- Lyapunov exponent, Ex. 15.11
- Strange attractor, Ex. 115.12

viewing the movie by Stewart (196?) and looking at photographs, e.g. in Van Dyke (1982). For the influence of boundary layers and turbulence on the flight of balls of various sorts, see Adair (1990), Armenti (1992), and Lighthill (1986). For the onset of turbulence, and more generally the onset of chaos in dynamical systems and mathematical maps, see Sagdeev, Usikov and Zaslavsky (1988), and Acheson (1990).

# Bibliography


Acheson, D. J. 1990. *Elementary Fluid Dynamics*, Oxford: Clarendon Press.

Adair, R. K. 1990. *The Physics of Baseball*, New York: Harper and Row.

Armenti, A., Jr., editor 1992. *The Physics of Sports*, New York: The American Institute of Physics.

Drazin, P. G. and Reid, W. H. 1981. *Hydrodynamic Stability*, Cambridge: Cambridge University Press.

Feigenbaum, M. 1978. "Universal behavior in nonlinear systems," *J. Stat. Phys.*, **19**, 25.

Gollub, J. P. 1980. "Many routes to turbulent convection," *J. Fluid. Mech.*, **100**, 449.

Landau, L. D. and Lifshitz, E. M. 1959. *Fluid Mechanics*, Reading, Massachusetts: Addison Wesley.

Libchaber, A. and Maurer, J. "Local probe in a Rayleigh-Bénard expriment in liquid helium," *Phys. Lett. Paris,* **39**, L369 (1978).

Lighthill, M. J. 1986. *An Informal Introduction to Theoretical Fluid Mechanics*, Oxford: Oxford Science Publications.

Lorenz, E. N. 1963. "Deterministic nonperiodic flow". *J. Atmospheric Sciences*, **20**, 130.

Ott, E. 1982. "Strange attractors and chaotic motions of dynamical systems" *Rev. Mod. Phys.*, **53**, 655.

Ott, E. 1993. *Chaos in Dynamical Systems*, Cambridge: Cambridge University press.

Sagdeev, R. Z., Usikov, D. A., and Zaslovsky, G. M. 1988. *Non-Linear Physics from the Pendulum to Turbulence and Chaos*, Harwood.

Stewart, R. W. 196?. *Turbulence*, a movie (National Committee for Fluid Mechanics Films); available at http://web.mit.edu/fluids/www/Shapiro/ncfmf.html .

Tanimoto, T. and Um, J. 1999. "Cause of Continuous Oscillations of the Earth," *J. Geophysical Research*, **104**, No. B12, pp. 28723–28739.

Tennekes, H. and Lumley, J. L. 1972. *A First Course on Turbulence*, Cambridge: MIT Press.

Tritton, D. J. 1977. *Physical Fluid Dynamics*, New York: Van Nostrand Reinhold.

Van Dyke, M. 1982. *An Album of Fluid Flow*, Stanford: Parabolic Press.

Verhulst, P. F. 1838. "Notice sur la loi que la population poursuit dans son accroissement," *Correspondance Mathématique et Physique* **10**, 113.

White, F. M. 1991. *Viscous Fluid Flow*, second edition, New York: McGraw Hill.